7-23-2015

Hydrologic Changes During the Middle Miocene in Southwestern Montana Using Molecular Biomarkers of Leaf Waxes

Jaclyn G. White
University of Connecticut - Storrs, jaclyn.white@uconn.edu

Hydrologic Changes During the Middle Miocene in Southwestern Montana Using Molecular Biomarkers of Leaf Waxes

Jaclyn White

B.S., Lafayette College, 2013

A Thesis

Submitted in Partial Fulfillment of the

Requirements for the Degree of

Master of Science

At the

University of Connecticut

2015

APPROVAL PAGE

Masters of Science Thesis

Hydrologic Changes During the Middle Miocene in Southwestern Montana Using Molecular Biomarkers of Leaf Waxes

Presented by

Jaclyn G. White, B.S.

Major Advisor_____

Michael Hren

Associate Advisor_____

Andrew Bush

Associate Advisor_____

Lisa Park Boush

University of Connecticut

2015

Acknowledgements

I would like to thank my thesis advisor Dr. Michael Hren for his guidance and time throughout this entire project. I would like to thank my other thesis committee members Dr. Andrew Bush and Dr. Lisa Park Boush for their insight and assistance. Finally, this project would not have been possible without the Geological Society of America and the University of Connecticut Center for Integrative Geosciences.

Table of Contents

Abstract

The Middle Miocene Climatic Optimum (MMCO) represents one of the most important large-scale CO_2-driven warming events of the Cenozoic and provides an opportunity to assess how global hydrological patterns are affected by increased warmth. This event was characterized by a global temperatures ~3-6 ºC warmer than modern averages and is equivalent to model predictions for climate change over the next century. We collected samples that span the MMCO event from Railroad Canyon and Hepburn's Mesa basins in southwest Montana to develop records of isotope hydrology during the MMCO. Specifically, this work uses the δD and $\delta^{13}C$ of terrestrial plant waxes and the δD of volcanic glasses to examine environmental change to this landscape during the MMCO.

The isotopic compositions of *n*-alkanes synthesized in plant leaf waxes preserve a record of paleoenvironmental conditions at the time of wax synthesis, including precipitation and plant water use efficiency. The δD and $\delta^{13}C$ values of *n*-alkanes were relatively invariant over the study interval except for two periods of synchronous enrichment occurring at ~15.0 and ~17.3 Ma. The isotopic compositions of volcanic glasses in rhyolitic ashes describe the original isotopes of precipitation at the time when ashes were produced. The δD of volcanic glasses slightly decreased over the study interval with two periods of enrichment occurring at ~15.0 and ~17.4 Ma. These data indicate variation in the moisture content and source of precipitation to basins in southwestern Montana during the Miocene. Episodes of heightened aridity paired with enrichment of source water were related to brief incursions of equatorial Pacific water into the

North Pacific. Data collected by this study suggest aridity and greater variability in precipitation will affect this region over the next century.

Introduction

An unresolved issue in predictions of future climate change is how global water resources will be affected by increasing mean annual temperature (MAT) and pCO_2 over the next century. Models can be useful tools for determining the effects of a warmer climate on the hydrologic cycle for many regions but they provide inconclusive predictions for precipitation changes in southwestern Montana and disagree upon fundamental points like whether moisture will increase or decrease per degree warming (Solomon et al. 2009). Alternatively, observations of hydrologic variation during ancient warm periods in Earth's history can be used as predictors for our future. Terrestrial sediments archive hydrologic changes through the preservation of biologically synthesized molecules with isotopic compositions indicative of the conditions of ancient environments (Peters et al. 2010). The δD and $\delta^{13}C$ compositions of leaf waxes are influenced by changes in hydrology and ecosystem taxa compositions and can be used to ascertain the paleohydrology of environments from the geologic past (Liu & Huang; 2005; Castañeda et al. 2007; Castañeda et al. 2009; Tipple & Pagani 2010; Tipple et al. 2011; Feakins et al. 2012; Feakins et al. 2013). This paper examines the isotopic composition of leaf waxes deposited in the Railroad Canyon and Hepburn's Mesa basins (southwestern Montana) in order to understand hydrologic patterns during the Middle Miocene and to predict hydrologic changes over the next century in this region.

Middle Miocene Climate

The MMCO is an interval of increased global temperatures occurring between 18.0 and 14.0 Ma. This warm interval preceded an abrupt cooling event that led to the first appearance of northern hemisphere glaciation in the Cenozoic and laid the foundations for modern climate dynamics (Figure 1) (Flower & Kennett 1994; Zachos et al. 2001). The MMCO is characterized by global MAT that is 3-6 ºC warmer than present and pCO_2 between 350-450 ppm, which is equivalent to the current pCO_2 of ~400 ppm and similar to predictions for MAT by the end of this century (Flowers & Kennett 1994; Sheldon 2006; Kurschner et al. 2008; Retallack 2009; You et al. 2009; Foster et al. 2012). Concurrent with the MMCO was the opening of the Drake passage and shifts in orbital imprinting of oxygen and carbon isotopes of benthic foraminifera, implying that warming during the Miocene was not solely a consequence of pCO_2 forcing but resulted from changes in ocean circulation patterns and meridional heat transport as well (Kennett 1977; Wright et al. 1992; Flowers & Kennett 1994; Pagani et al. 1999; Royer et al. 2001; Holbourn et al. 2007; Holbourn et al. 2013). Regardless of the cause of the MMCO, the consequences of high temperatures and high pCO_2 for the biota were conspicuous, including evolutionary turnover of benthic and planktonic foraminifera and the appearance and expansion of C_4 grasslands (Woodruff 1985; Wei & Kennett 1986; Flowers and Kennett 1994; Wolfe 1985; Strömberg & McInerney 2011).

The MMCO was followed by rapid cooling starting at ~14.5 Ma (Flowers and Kennett 1994; Pagani et al. 1999; Zachos et al. 2001). Triggers for the middle Miocene cooling are contested with hypotheses ranging from atmospheric CO_2 draw down through heightened burial

of organic carbon, to enhanced marine productivity was related to greater silicate weathering and nutrient flux lowering global temperature (Vincent & Berger 1985; Hodell & Woodruff 1994; Raymo 1994; Pearson & Palmer 2000). Mounting evidence of 100-Ka and 60-Ka periodicity of the growth and retreat of the East Antarctic Ice Sheet beginning at ~14 Ma indicate that orbital tuning that may have prompted the shift to cooler global temperatures towards the close of the Miocene (Miller et al. 1991; Wright et al. 1992; Shevenell et al. 2004; Holbourn et al. 2007; Holbourn et al. 2013).

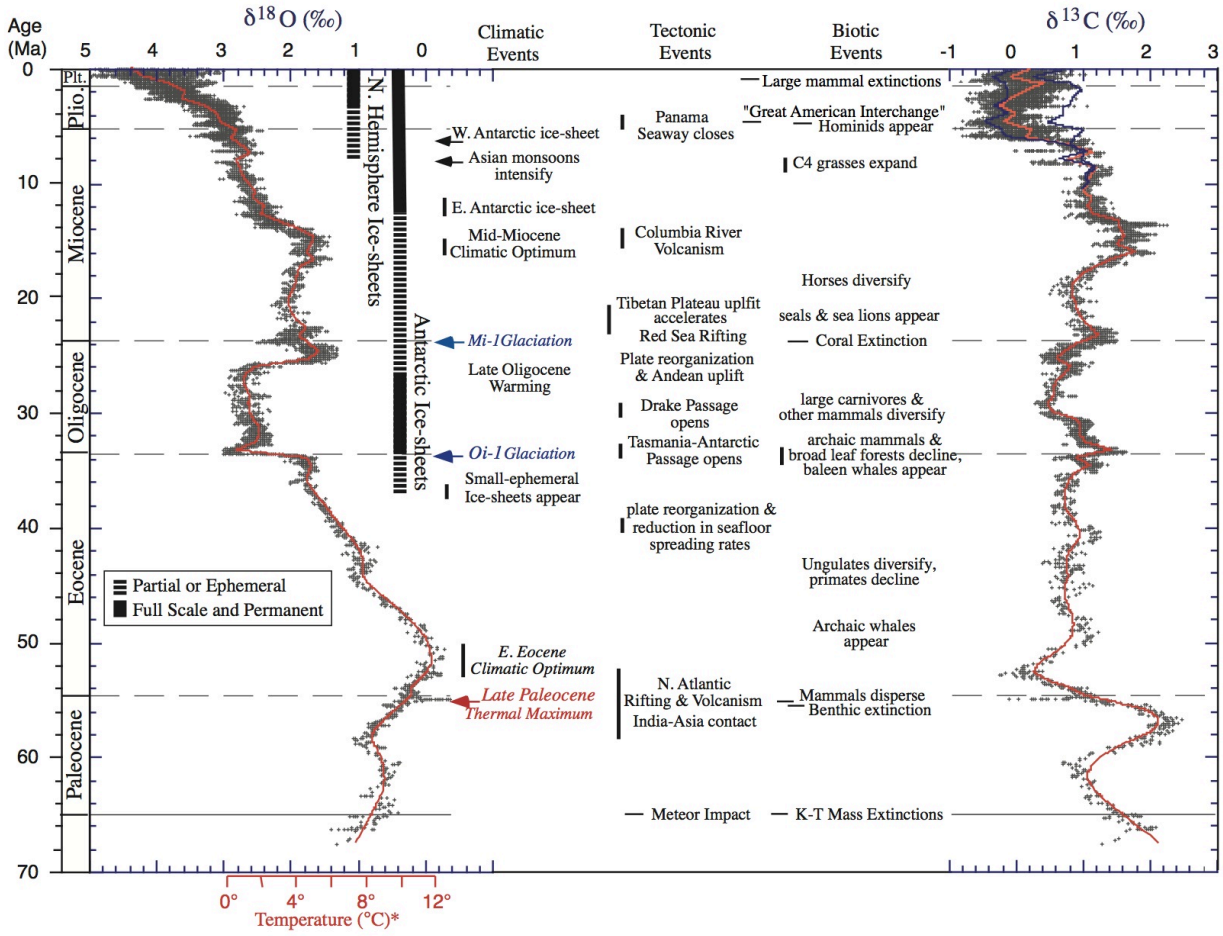

Fig. 1: $\delta^{13}C$ and $\delta^{18}O$ of benthic foraminifera from the past 65 Ma (reproduced from Zachos et al. 2001).

The MMCO was the warmest period in Earth's history since the Eocene and the uplift of the Rocky and Himalayan mountain ranges (Flowers & Kennett 1994; Zachos et al. 2001; Horton et al. 2004; Graham et al. 2005; Kent-Corson et al. 2006; Rowley & Currie 2006). Molecular biomarkers preserved within sediments deposited during the Miocene offer a unique opportunity to examine hydrologic changes that happened in conjunction with warmer global temperature within the context of modern tectonic configurations.

Geologic History of Railroad Canyon and Hepburn's Mesa

Railroad Canyon and Hepburn's Mesa are coeval Miocene sections deposited in intermontane basins that developed in conjunction with the Laramide Orogeny and Yellowstone hotspot volcanism during the early to middle Cenozoic (Barnosky & Labar 1989; Kent-Corson et al. 2006; Barnosky et al. 2007). These sedimentary basins exist along the eastern edge of the North American Cordillera that was uplifted as a result of the collision and subduction of the oceanic Farallon plate beneath the North American plate beginning ~170 Ma during Jurassic time (Figure 2). Early tectonism contributing to Cordilleran uplift deformed sediments during the Nevadan Orogeny, creating island and volcanic arcs off the western coast of the North American plate (Coney 1987). During late Early Cretaceous time, the North American plate overran the Farallon plate, resulting in low-angle subduction and crustal uplift occurring further inland, deforming and uplifting sediments in the Sevier thrust belt (Miller & Gans 1989; DeCelles 2004). The final phase of uplift happened during the early Cenozoic and was characterized by sweeping magmatism from north to south and uplift of metamorphic core

complexes across the Rocky Mountains (Coney & Harms 1984; DeCelles 2004; Kent-Corson 2006). Following this phase of uplift, sediments within the region experienced deformation as Yellowstone hotspot activity initiated. Broad intermontane basins were compressed into the narrow valleys present in the region today, and sediments deposited in the basin were supplemented by rhyolitic ash falls produced via Yellowstone volcanism (Lonn et al. 2000; Kent-Corson 2006; Sears et al. 2009).

The Hepburn's Mesa Formation was deposited within the Yellowstone Valley half-graben situated between the Gallatin and Beartooth Ranges and are bounded by the Suce Creek fault to the north, the Gardiner fault to the south, and the Deep Creek and Luccock Park faults to the

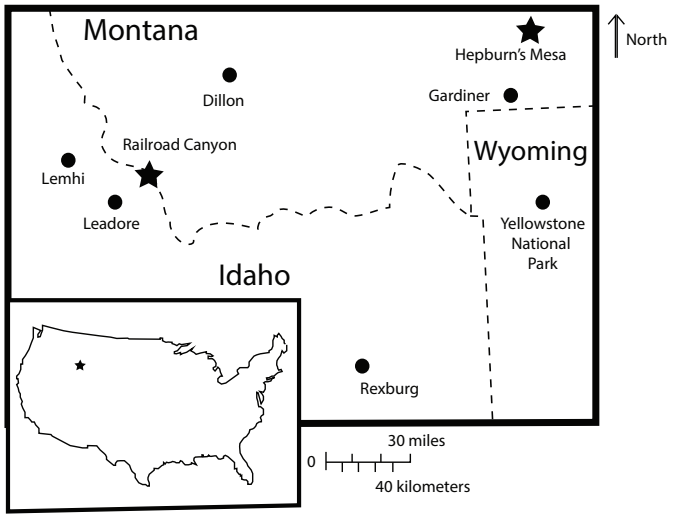

Fig. 2: Site locations where samples for this study were collected from at Railroad Canyon and Hepburn's Mesa.

east. The orientation of the half-graben and faults within the valley indicate the basin developed in conjunction with basin and range province tectonism and Yellowstone volcanism beginning in the early Miocene (Barnosky & Labar 1989; Sears et al. 2009). The Hepburn's Mesa Formation spans 16-14.8 Ma based upon the presence of Early and Late Barstovian fauna and magnetostratigraphic correlations (Figure 3). These fossils include *Spermophilus sp., saMesogaulus douglassi, Proheteromys sp., Peridiomys sp., Lignimus sp., Mojavemys sp., Pseudotheridomys sp., Schaubeumys sp., Camelidae sp., Dromomeryx sp., Parahippus sp., and Hypohippus sp.* (Barnosky and Labar 1989). Sediments within the basin are composed of thinly laminated white, pink, and green mudstones, siltstones, sandstones and ashes spliced by an east-dipping normal fault. Minerals including halite, calcite, and clinoptilolite are abundant throughout the section and suggest deposition occurred within a periodically saline, shallow perennial lake system. Intermittently present mudcracks and insect burrows indicate mudflat deposition also occurred within the arid Hepburn's Mesa paleoenvironment. A thick conglomerate layer unconformably lies above the Hepburn's Mesa Formation and is capped by two Pliocene basalt flows (Montagne et al. 1982; Barnosky & Labar 1989). The arid nature of the Hepburn's Mesa depositional environment is reflected by the geomyoid rodent fossils, evaporite minerals, and sedimentological features distributed within the section (Barnosky and Labar 1989).

Railroad Canyon sediments were deposited within an intermontane basin of the Beaverhead Mountains of Montana and Idaho, which were created during the final phase of Cordilleran uplift during the Laramide Orogeny in the early Cenozoic. Oxygen isotopes of pedogenic carbonates from Railroad Canyon and nearby basins show that Laramide uplift

affected the region during the early Eocene and that topography has not substantially changed since then (Kent-Corson et al. 2006).

Late Hemingfordian and Barstovian age vertebrate fossils are common in the Railroad Canyon basin. Magnetostratigraphy of sediments from the basin correlate with chrons 5D through 5A and provide estimates for timing of deposition between 17.6-12.99 Ma (Figure 3) (Barnosky et al. 2007). Dentaries of several ancient mammals have been recovered from the basin including *Tylocephalonyx skinneri, Acritohippus isonesus, Hypohippus sp., Archaeohippus ultimus, Brachycrus sp., Ticholeptus zygomaticus, Merychyus sp., Aepycamelus sp., Paramyolabis sp., Bouromeryx sp., Rakomeryx sp., Paracosoryx wilsoni, Pliocyon sp., Hypolagus sp., Oreolagus sp., Alphagaulus vetus, Mesogaulus sp., Plesiosminthus sp., Harrymys irvingi, Peridiomys sp., and Cupidinimus sp.* (Barnosky et al. 2007). The ancient mammal fossils found in Railroad Canyon are ancestors to modern mammals that inhabit prairie environments and indicate a semi-arid climate in the basin during the Miocene which is corroborated by lithologic evidence.

The Railroad Canyon Sequence includes the sedimentary Renova and Six Mile Creek formations, which are frequently interbedded with volcanic ashes supplied by Yellowstone volcanism beginning in the early Miocene (Kent-Corson et al. 2006; Sears et al. 2009). The Mid-Tertiary Unconformity (MTU), a prominent stratigraphic feature apparent in several basins along the eastern extent of the Rocky Mountains, separates the finer-grained Renova Formation from the coarser-grained Six Mile Creek Formation and is a regionally useful marker separating earlier Miocene fauna from later Miocene fauna (Kent-Corson et al. 2006; Barnosky et al. 2007; Sears et al. 2009). The Renova Formation is composed of fine-grained white, tan, and green

mudstones and siltstones and a increasing abundance of mudcracks up to the MTU. These sediments are replaced by pink and tan sandstones and poorly-sorted conglomerates with abundant gravels and cobbles above the MTU. The lithologic change observed in the Railroad Canyon section implies a shift in depositional settings from lacustrine and river channel sediments to aeolian and mudflow deposition that corresponds with aridification of the Miocene environment. These variations in the depositional setting and lithology of sediments in Railroad Canyon were likely precipitated by tectonic and climatic changes occurring simultaneously (Barnosky et al. 2007).

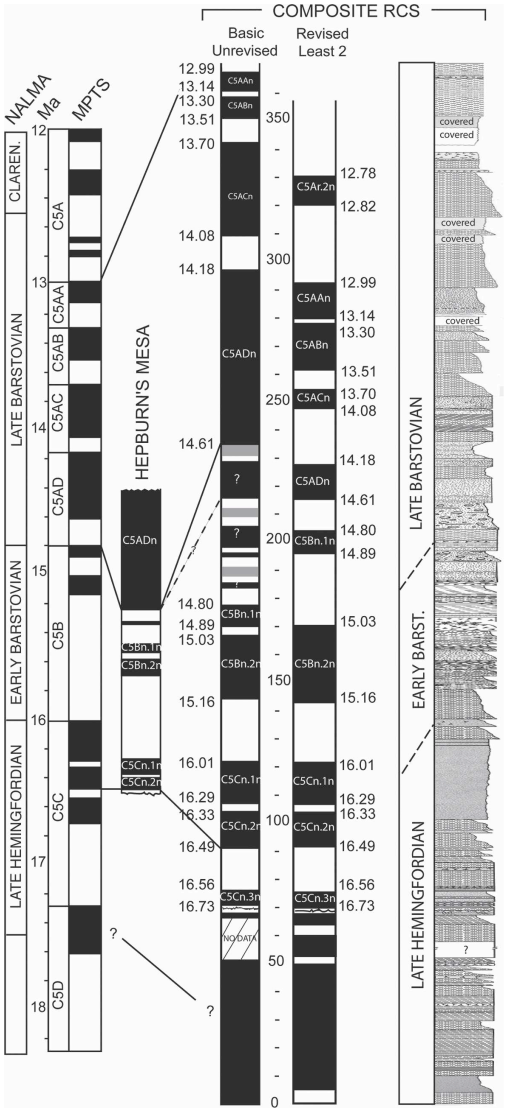

Fig. 3: Magnetostratigraphic corelations between Railroad Canyon and Hepburn's Mesa (modified from Barnosky et al. 2007).

Small-scale epiorogenic uplift concurrent with the MTU and related to movement and activity of the Yellowstone hotspot mildly compressed sediments with a northwest-southeast orientation. Compression altered the shape of the Railroad Canyon basin by opening the drainage environment of the previously closed lacustrine setting and can account for the larger grain sizes observed in sediments above the MTU (Kent-Corson et al. 2006; Barnosky et al. 2007). The MTU also overlaps temporally with the beginning of the MMCO and suggests that

coarsening lithology and aridification were also influenced by hydrologic changes in the basin associated with a global warming event (Zachos et al. 2001; Barnosky et al. 2007). Tectonic controls of aridification can be separated from hydrologic controls by examining the isotopic composition of leaf waxes preserved in sediments from the basin and can quantify paleoenvironmental changes associated with the MMCO.

Normal Alkanes

n-alkanes are straight-chain, saturated hydrocarbons that are derived from the epiticular waxes of terrestrial plants and serve to reduce non-stomatal water loss, protect against ultraviolet radiation, and defend against herbivory. They coat the outer surface of aerial plant tissues and can be preserved in soil after the plant decomposes (Eglinton & Hamilton 1967; Bianchi & Canuel 2011). These compounds are useful as biomarkers because they record δD and $\delta^{13}C$ signals of the environment at the time of leaf wax synthesis during leaf flush, a two-week period following leaf budding when waxes are created, incorporating hydrogen and carbon isotopes from the environment (Figure 4) (Tipple et al. 2012).

Plant synthesized *n*-alkanes are distinguishable from other waxes because they are longer and have a greater abundance of odd rather than even chain lengths. These characteristics are imparted on plant synthesized *n*-alkanes during leaf waxes synthesis. During leaf wax synthesis, even-chain fatty acids elongate to produce compounds composed of 20-34 carbons by the repetitive addition of the 2 carbon unit malonyl-ACP (Zhou et al. 2010). Following extension, even-chain fatty acids react through disparate pathways to form a range of compounds all present

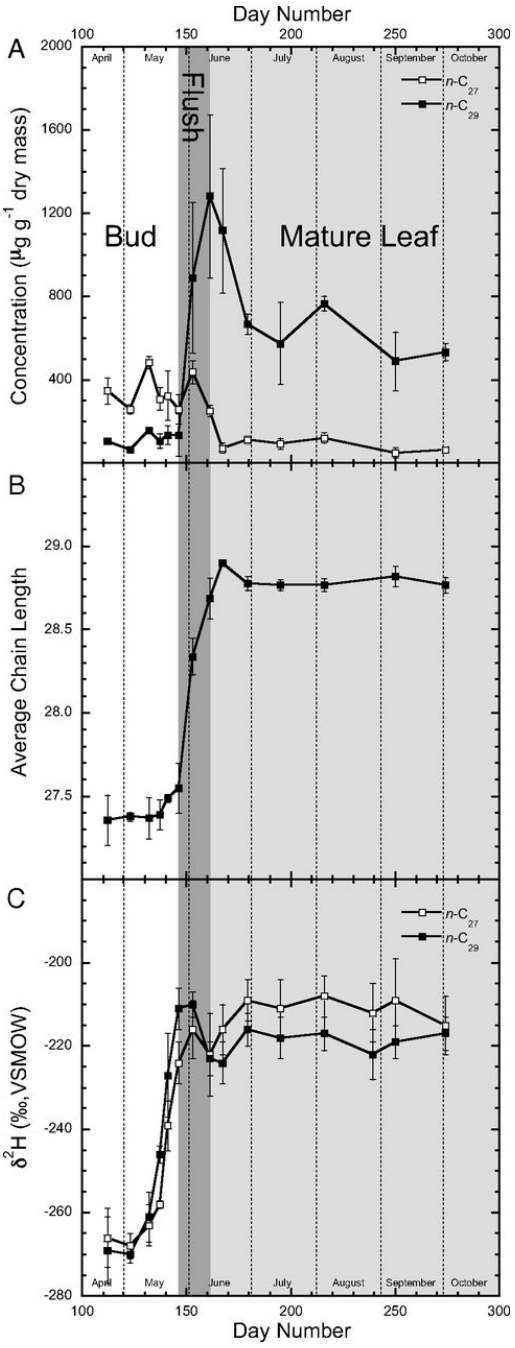

Fig. 4: Modern studies of the deciduous angiosperm *P. angustifolia* show A) distribution of *n*-alkane chain lengths during early spring, following budding, and later in the growing season. B) extension of *n*-alkane chain lengths during the year and C) δD values of *n*-alkanes throughout the growing season (taken from Tipple et al. 2012).

in plant waxes including aldehydes, alkanes, primary and secondary alcohols, and ketones. Alkanes are created by the removal of a carboxyl group from even-chain number fatty acids within the decarbonylation pathway (Figure 5). Because of this, alkanes produced during leaf wax synthesis are dominantly odd-carbon chain lengths (Kunst 2003). An unresolved issue in the synthetic pathways of plant wax alkanes is the less abundant presence of even-chain alkanes. Even-chain number alkanes tend to be depleted in ^{13}C, enriched in D, and are much less common compared to their odd-chain counterparts. Based on their isotopic compositions, it has been proposed that even-chain alkanes are derived from the formation of propionate following the reduction of pyruvate. However, studies determining the origin of even-chain number alkanes are limited (Zhou et al. 2010).

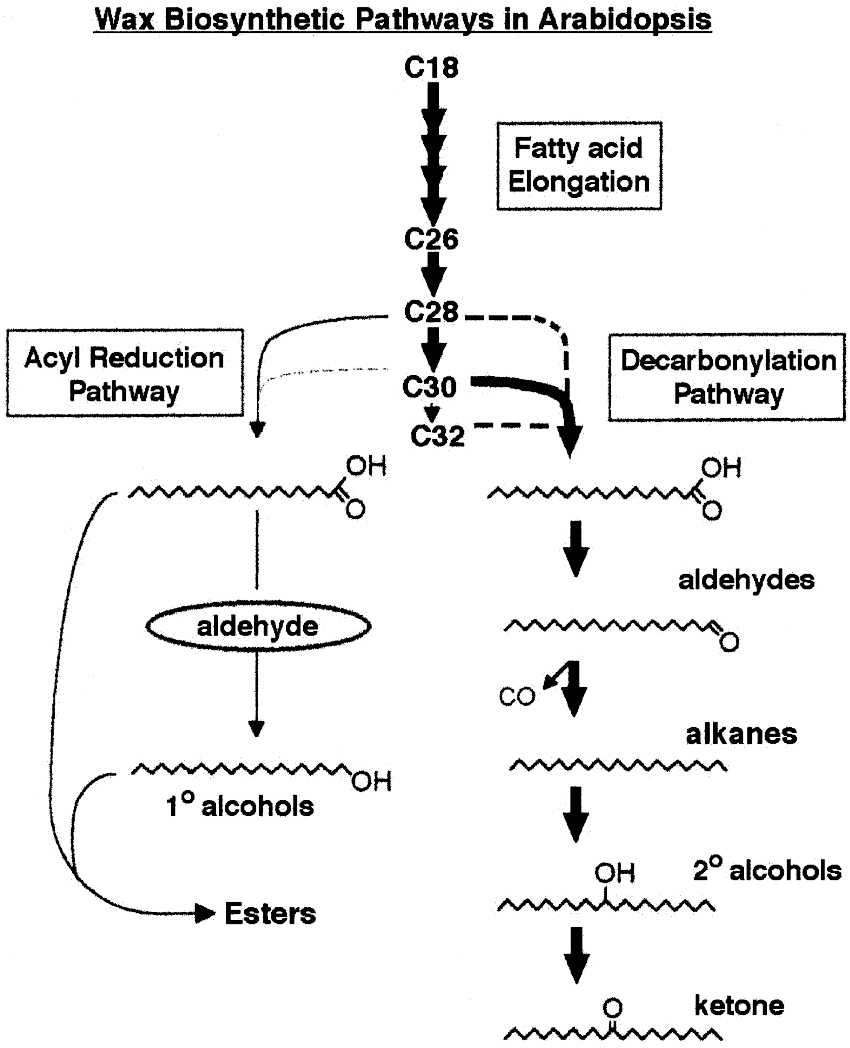

Fig. 5: Biosynthetic pathways of plant wax synthesis following fatty acid elongation (taken from Kunst 2003).

Processes Affecting δD of n-alkanes

The factors controlling the δD values of leaf waxes are δD of precipitation, relative humidity, and the composition of the vegetation (Hou et al. 2008). The δD of precipitation is related to the latitude and topography of the environment. Global precipitation originates from atmospheric moisture derived from low-latitude regions where original isotopic composition is

determined by equilibrium fractionation of isotopes between the atmosphere and the ocean. Through Rayleigh distillation, the isotopic composition of precipitation becomes more depleted as water vapor moves from low to high latitudes, across a continent, or over a topographic high (Bowen & Revenaugh 2003). Adiabatic cooling of rising air masses over mountain slopes causes rainout on the windward sides of mountains to be isotopically enriched and the leeward sides to be isotopically depleted (Gat 1996).

The δD of precipitation typically controls the isotopic signature of water in an ecosystem before it is incorporated into leaf wax *n*-alkanes (Hou et al. 2008). Prior to leaf wax synthesis, water isotopes are fractionated by evaporation of isotopically lighter hydrogen from the soil. The rate of soil evaporation is influenced by the relative humidity of an environment, and extensive evaporation of soil water will result in isotopically enriched δD values. Once captured from the soil, water isotopes are fractionated by transpiration within the leaf of the plant (Figure 6) (Gat 1996; Sachse et al. 2006; Tipple & Pagani 2013). The magnitude of fractionation through transpiration varies by plant functional type; for example, grasses tend to be ~50‰ lighter than trees and woodland plants due to differences in the stomatal regulation and leaf architecture of the different species (Tipple & Pagani 2007; Hou et al. 2008). Environmental conditions also affect the rate of leaf transpiration. Sachse et al. (2004) assessed the magnitude of fractionation from soil water and leaf water by comparing the δD of leaf waxes from terrestrial plants and aquatic plants living within and around a lake. Their results revealed a 10-60‰ difference between the two environments, given that the biosynthetic fractionation of all plants were equal. This allowed them to estimate the combined effects of evapotranspiration from the soil and leaf

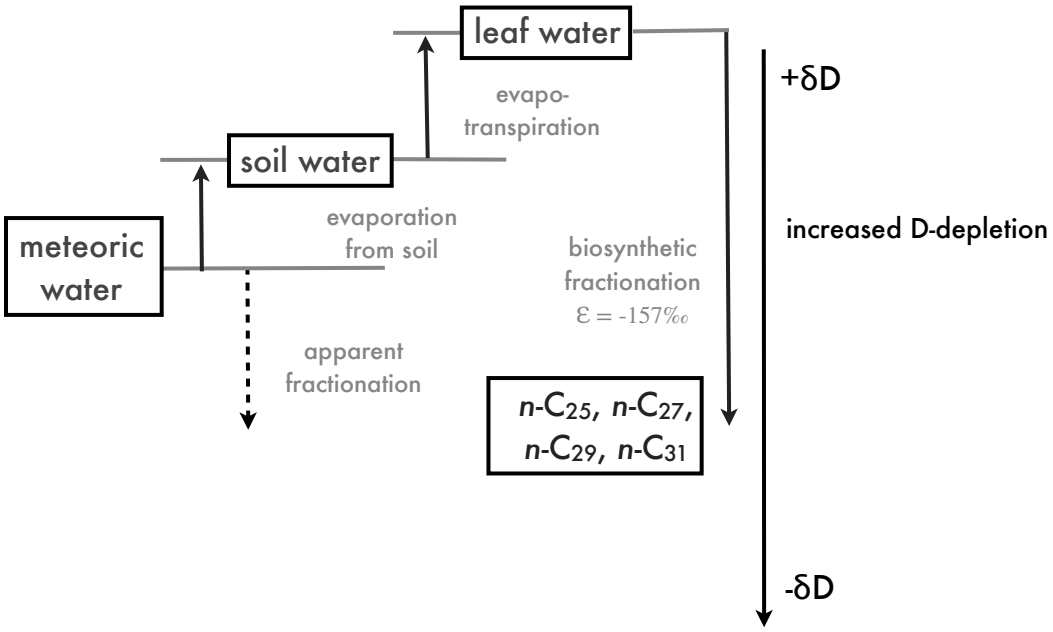

Fig. 6: Changes in isotopic composition of meteoric water as it is fractionated through evaporation, evapotranspiration, and biosynthetic fractionation before being taken up by plant wax n-alkanes (modified from Sachse & Samuels 2006).

stomata and determine the apparent fractionation ($\varepsilon_{apparent}$); a measurement of the evaporative effects of an environment (Sachse et al. 2004).

Biosynthetic fractionation occurs as hydrogen is taken from leaf water and incorporated into leaf waxes. All plant species preferentially select isotopically light hydrogen to be incorporated within waxes but differ in the extent of fractionation. For example, biosynthetic δD fractionation is strongly influenced by plant functional type. Leaf waxes of C_3 plants are ~30‰ more enriched than leaf waxes of C_4 plants due to differences in leaf structure and pathways of NADPH formation during synthesis. Furthermore, within C_3 plants, dicotyledons are enriched

by ~36‰ compared with monocotyledons as they differ in the timing and location of wax synthesis in the leaves (Chikaraishi & Naraoka 2003; Sachse et al. 2012; Tipple & Pagani 2013). While differences in plant functional type exert a strong influence on δD of leaf waxes, modern studies suggest soils integrate hydrologic signals of leaf waxes from entire ecosystems and that *n*-alkanes preserved in sediments accurately portray environmental signals (Tipple & Pagani 2010).

Processes Affecting $\delta^{13}C$ of n-alkanes

The $\delta^{13}C$ composition of leaf wax *n*-alkanes is primarily influenced by the isotopic composition of atmospheric CO_2 at the time of leaf wax synthesis. Stomatal regulation and carbon discrimination between plant functional types also influence the $\delta^{13}C$ of leaf waxes. C_3 and C_4 plants utilize distinct processes during carbon fixation, resulting in C_4 plants having more isotopically enriched $\delta^{13}C$ values of leaf waxes. In fact, early studies seeking to understand the differences between C_3 and C_4 pathways in plants exploited these divergent isotopic compositions as pathway tracers (Wickman 1952; Craig 1953). The C_3 photosynthetic pathway is the evolutionarily more primitive pathway. In this process, inorganic carbon diffuses into the mesophyll and is fixed by RuBisCo during the generation of ATP through the Calvin-Benson cycle. While differential diffusivity of $^{12}CO_2$ and $^{13}CO_2$ affects the subsequent isotopic composition of leaf waxes, $\delta^{13}C$ is more strongly affected by carbon discrimination during fixation by RuBisCo (Farquhar et al. 1989). ^{13}C is discriminated against during carbon fixation, resulting in average isotopic values of $\delta^{13}C$ of C_3 leaf waxes between -20‰ and -35‰. C_4 plants

developed a biologic pump in order to enhance the efficiency of the Calvin-Benson cycle. Prior to carbon fixation by RuBisCo, CO_2 diffused within the mesophyll is converted to bicarbonate and picked up by PEP carboxylase (Figure 7). PEP carboxylase has a greater affinity for ^{13}C than Rubisco, resulting in isotopically heavier $\delta^{13}C$ of C_4 bulk carbon and leaf waxes (Figure 8) (Farquhar 1989; Tipple & Pagani 2007).

In modern and paleoenvironmental studies the $\delta^{13}C$ of leaf waxes can be useful for determining past hydrology so long as atmospheric CO_2 and C_3/C_4 plant compositions are well

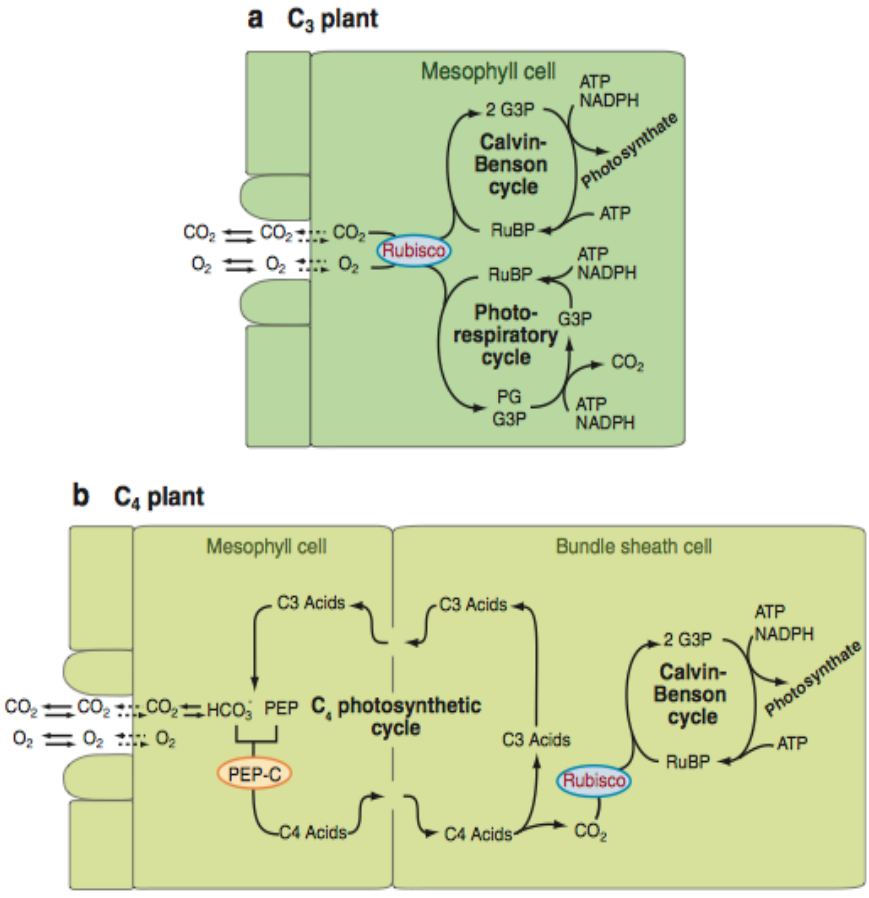

Fig. 7: Photosynthetic pathways of a) C_3 plants and b) C_4 plants (taken from Tipple & Pagani 2007).

constrained. Water-loss regulation, integral during times of low relative humidity, influences the $\delta^{13}C$ of leaf waxes. Plants open their stomata in order to obtain CO_2 for metabolism but lose H_2O during this process. In times of environmental aridity, stomata are open for shorter intervals in order to prevent water loss. During times of increased moisture, stomata are open for longer as water stress is not as high. Because of this, CO_2 concentration within stomata is greater during times of increased moisture and there is greater discrimination against ^{13}C. During times of decreased moisture, the CO_2 concentration within stomata is lower and there is less carbon discrimination as production of ATP is prioritized over isotopic carbon composition. Relative humidity and pCO_2 oppositely influence the $\delta^{13}C$ of leaf waxes. Plants can acquire sufficient CO_2 for metabolic process over shorter intervals during times of high pCO_2, complicating

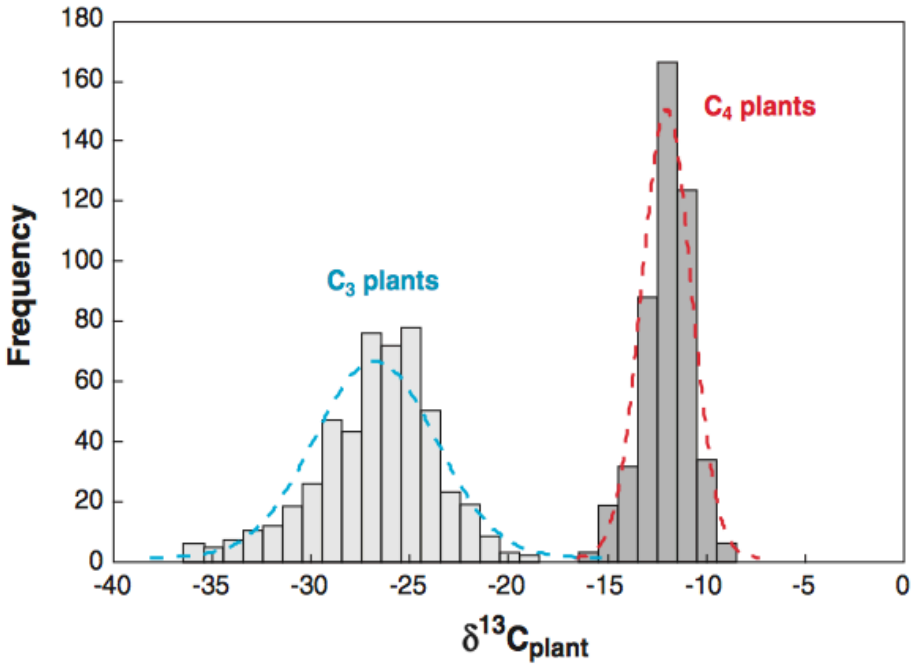

Fig. 8: Normal distributions of bulk C_3 and C_4 plant isotopic values (taken from Cerling et al. 1999).

hydrological signals based upon isotopic carbon composition (Farquhar & Sharkey 1982; Tipple & Pagani 2007).

Processes Affecting Average Chain Length (ACL)

The determination of *n*-alkane chain lengths is useful for ascertaining paleoenvironmental conditions and helps to delineate between different classes of plants exuding epiticular waxes. The ACL is measured using the equation:

$$ACL = \frac{25(A_{25}) + 27(A_{27}) + 29(A_{29}) + 31(A_{31}) + 33(A_{33})}{A_{25} + A_{27} + A_{29} + A_{31} + A_{33}}$$

where A is equal to the area of the peak from a gas chromatograph analysis. Terrestrial plants produce *n*-alkanes with chain-lengths between C_{25}-C_{33} through fatty acid elongation during leaf wax biosynthesis (Eglinton & Hamilton 196l; Zhou et al. 2010). Modern plants show a positive relationship between *n*-alkane ACL and MAT and an inverse relationship with latitude. While no cause and effect relationship has been shown, longer chain lengths may better prevent leaf desiccation and are thought to be indicative of warmer, drier conditions (Gagosian & Peltzer 1986; Schefuß et al. 2003; Sachse et al. 2004; Tipple & Pagani 2007).

Several studies have revealed substantial differences in ACL patterns of *n*-alkanes between plants inhabiting the same ecosystems which can be attributed to differences in plant functional types within a plant communtiy (Sachse et al. 2006; Tipple & Pagani 2013). Subjected to similar environmental conditions, plants using the C_4 photosynthetic pathway synthesize longer chain alkanes than plants using the C_3 pathway. While the explanation for the

relationship between ACL and environment is speculative, the evolutionary advantages of C_3/C_4 pathways and the environment are well understood. C_4 plants possess physiological advantages during periods of low pCO_2 and times of environmental aridity that allow them to obtain CO_2 while limiting transpiration (Farquhar 1989; Tipple & Pagani 2010). Therefore, elongation of soil extracted *n*-alkanes can be interpreted as the consequence of paleoenvironmental shifts to warmer and/or drier climates.

n-Alkane Resistance to Thermal Degradation

The δD, $\delta^{13}C$, and ACL of *n*-alkanes depend upon paleoenvironmental conditions of temperature and water availability during the time they were produced. The chemical stability and non-polarity of *n*-alkanes suggest that these paleoenvironmental signals are preserved over geologic time. Hydrogen atoms covalently bonded to carbon atoms do not readily exchange with surrounding water molecules at shallow burial temperatures below ~150 ºC and experience a slower rate of hydrogen exchange with surrounding water than any other organic material (Figure 9) (Sessions et al. 2004; Pedentchouk et al. 2006; Schimmelmann 2006). However, with increased diagenesis and throughout catagenesis (R_o greater than 0.4), δD values of *n*-alkanes become more enriched compared to the original composition, with the most enrichment occurring when the isotopic difference between soil organic matter and surrounding water is greatest (Schimmelman et al. 2006).

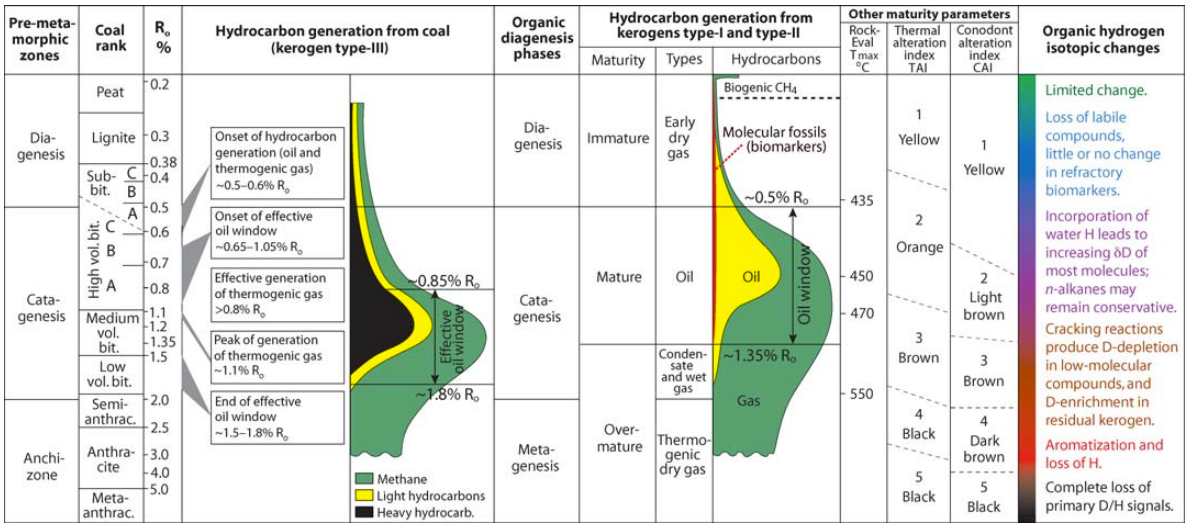

Fig. 9: Relationship between diagenesis and H exchange of organic material. *normal* alkanes retain their original δD composition through the early stages of diagenesis (taken from Schimmelmann et al. 2006)

Introduction to Paleoenvironmental Reconstructions from Volcanic Glasses

Volcanic glasses are produced as amorphous silicate shards within rhyolitic tuffs. Initially, they are composed of 0.1-0.3% magmatic water by weight but rapidly become fully hydrated by environmental water on the order of 1-10 Ka, depending upon the temperature, relative humidity, and composition of the glass (Friedman et al. 1993). Fully hydrated volcanic glasses are 3-8% water by weight (Friedman et al. 1993; Mulch et al. 2008; Dettinger 2013). Hydration of volcanic glass occurs through the process of osmosis and is driven by geochemical differences between glass and surrounding ambient water. Hydrogen atoms are preferentially bound to the glass structure over deuterium and empirical studies have determined this occurs with a fractionation factor of 1.034 (Friedman et al. 1993; Dettinger 2013). Following hydration, minimal hydrogen isotopic exchange with environmental water occurs at surface temperatures as there is a smaller diffusion gradient between the glass and water (Friedman et al. 1993; Mulch et

al. 2008; Dettinger et al. 2013). Fully hydrated volcanic glass provides a geologically robust record of the δD of environmental water at the time of ash fall and are useful for paleoaltimetry and paleoenvironmental reconstructions of precipitation (Friedman et al. 1993; Mulch et al. 2008; Cassel et al. 2012; Dettinger 2013).

Methods

Sample Collection

Sixteen lithified siltstones, sandstones, and mudstones were collected during the summer of 2009 and thirty-eight lithified siltsones, sandstones, mudstones and eleven ashes were collected during the summer of 2014 from the Railroad Canyon basin in order to characterize the hydrologic environment of the Middle Miocene in southwestern Montana. Nine lithified siltstones, mudstones and 1 ash were obtained from the Hepburn's Mesa Formation in southern Montana located ~209 kilometers northeast of Railroad Canyon. Samples were collected at the meter scale and compared to biostratigraphic and magnetostratigraphic data taken from Barnosky and Labar (1989) and Barnosky et al. (2007). All topsoil and outer layers of sediment cover were removed prior to collection in an effort to minimize the effects of modern weathering.

Sample Extraction and Preparation of n-alkanes

Samples were dried for 24-48 hours using a Labconco freeze dryer and extracted using an azeotrope of DCM:MeOH as solvent (2:1 v/v). Samples were dried under clean N_2 and separated by silica gel chromotography in ashed pasteur pipettes. Total lipid extracts were separated into three fractions, and the non-polar hydrocarbon fractions were eluted using 2 mL of hexane. When necessary, cyclic and branched hydrocarbons were separated from straight-chained, saturated alkanes using urea adduction.

Compound integrities and abundances were analysed using a Thermo Trace GC Ultra fitted with a flame ionization detector and a fused silica DB-1 phase column (60 m x 0.25 mm I.D., 0.25 μm film thickness). Helium was used as the carrier gas with flow of 2 mL/min. Compounds in hexane were injected split/splitless at 260 ºC and oven temperature ramped from 50 ºC-250 ºC at 15 ºC/minute, 250 ºC-320 ºC at 6 ºC/minute and held for 8 minutes. All sample traces were compared to known *n*-alkane standards and elution times.

Sample Extraction and Preparation of Volcanic Glasses

Powdered ashes were separated with brass sieves to obtain the 60-120 mesh fraction. These fractions were rinsed with deionoized water and decanted three times before being successively sonicated with 10% HNO_3 and 5% HF for 5 minutes each. Samples were dried in an oven at 60 ºC before hydrated glass was separated from magnetic and non-magnetic grains by repeated passes through a Frantz Isodynamic Separator. The purities of samples were confirmed with X-ray diffraction.

$\delta^{13}C$ and δD Analyses of n-alkanes

$\delta^{13}C$ and δD values of samples were measured using a Trace GC Isolink coupled to a Delta V Plus Mass Spectrometer. GC ramp, column conditions, and carrier flow were identical to those listed above.

Peaks were selected and integrated using IsoDat software. The H_3^+ factor was determined daily before hydrogen analysis and averaged 6.1 for analyses. Peaks were corrected for area, daily drift of the instrument, and offset from known standards provided by Arndt Schimmelman, Indiana University (Mix A5), which were run at various concentrations throughout the day.

Isotopic compositions of samples are written in delta notation, where

$$\delta = \left(\frac{R_{sample} - R_{std}}{R_{std}} \right) - 1$$

and R_{sample} is equal to the ratio of the heavy to the light isotope of either hydrogen or carbon of measured samples and reported relatve to the Vienna Pee Dee Belemnite Standard and Vienna Standard Mean Ocean Water.

δD Analyses of Volcanic Glasses

Samples were enclosed in silver foil and dried under vacuum prior to δD analysis by pyrolysis using a Thermo Electron TC-EA coupled to a Delta V Mass Spectrometer. Peaks were selected and integrated using IsoDat software. The H_3^+ factor was determined daily before analysis. Peaks were corrected for area, daily drift of the instrument, and offset from laboratory standards including KGA-2, PEF1, and NBS22. NBS22 was run at various concentrations and each standard was run several times throughout the day.

Isotopic compositions of samples are written in delta notation.

Results

Molecular Distributions of n-alkanes

Previous studies show sediments in Railroad Canyon span 17.6-12.99 Ma. Of the thirty-eight samples collected, eleven yielded concentrations of *n*-alkanes measurable using isotope ratio mass spectrometry. Previous studies show sediments collected from Hepburn's Mesa span 15.96-14.79 Ma and all nine samples collected were measurable using isotope ratio mass spectrometry.

The carbon preference index (CPI) measures the odd over even predominance of *n*-alkanes in a sample. As terrestrial plants synthesize *n*-alkanes with a greater abundance of odd rather than even chain lengths, compounds with CPI less than 1 are indicative of catagenesis and thermal degradation. The CPI of all samples analyzed in this study are greater than 1 and were calculated using the equation:

$$CPI = \frac{\left(A_{23} + A_{25} + A_{27} + A_{29} + A_{31} + A_{33}\right) + \left(A_{25} + A_{27} + A_{29} + A_{31} + A_{33} + A_{35}\right)}{2 * \left(A_{24} + A_{26} + A_{28} + A_{30} + A_{32} + A_{34}\right)}$$

For Railroad Canyon samples, CPI ranges between 1.4 and 4.9. The range of CPI values for samples collected from Hepburn's Mesa is 4.9 and 14.9. There is no correlation between depth and CPI for either site.

The ACL indicates the plant sourcing and environmental conditions of a sample. The ACL of samples collected from Railroad Canyon vary between 28.2 and 29.4 with an average of 28.6 (Figure 10). The ACL at Railroad Canyon does not change substantially through section

except between 17.43 and 16.90 Ma, when it increases by 1.2, and at 15.0 Ma, when it increases by 0.9.

The ACL of samples from Hepburn's Mesa varies between 29.4 and 30.1 with an average of 29.7 (Figure 11). The greatest shift of values occurs between 15.3 and 15.2 Ma when the ACL decreases by 0.5. By 14.8 Ma, the ACL of samples has returned to the mean value.

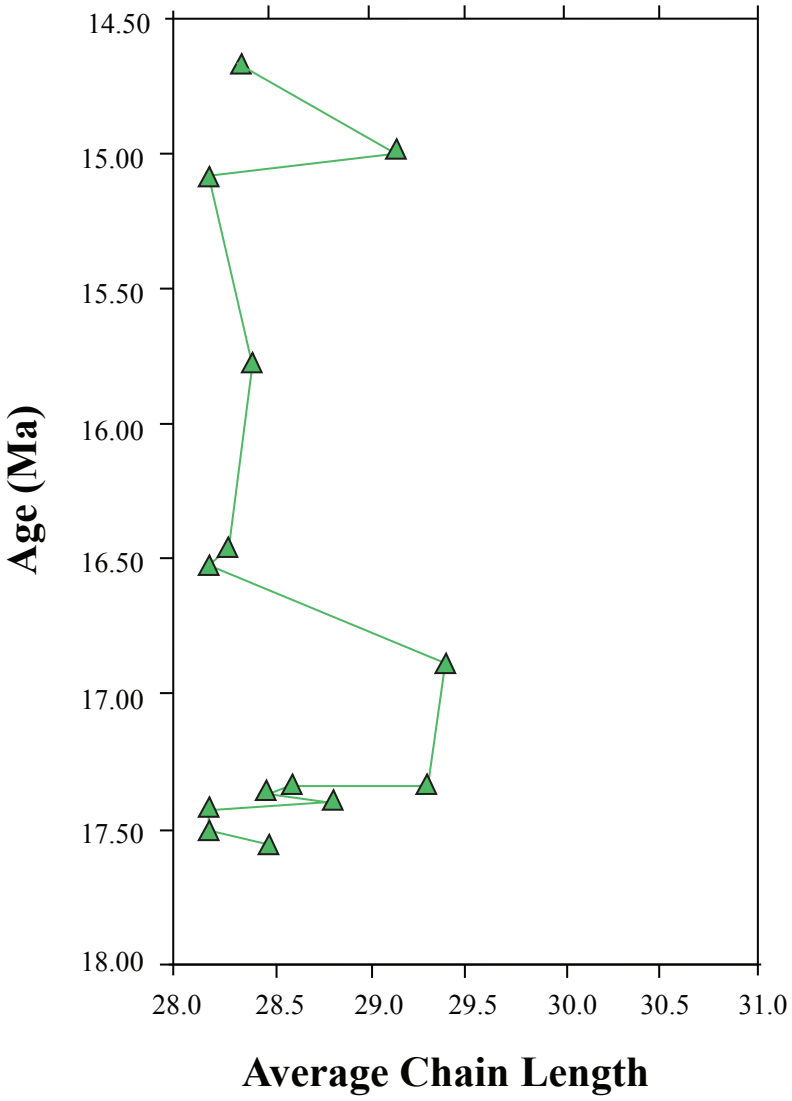

Fig. 10: ACL of *n*-alkanes extracted from sediments deposited in Railroad Canyon.

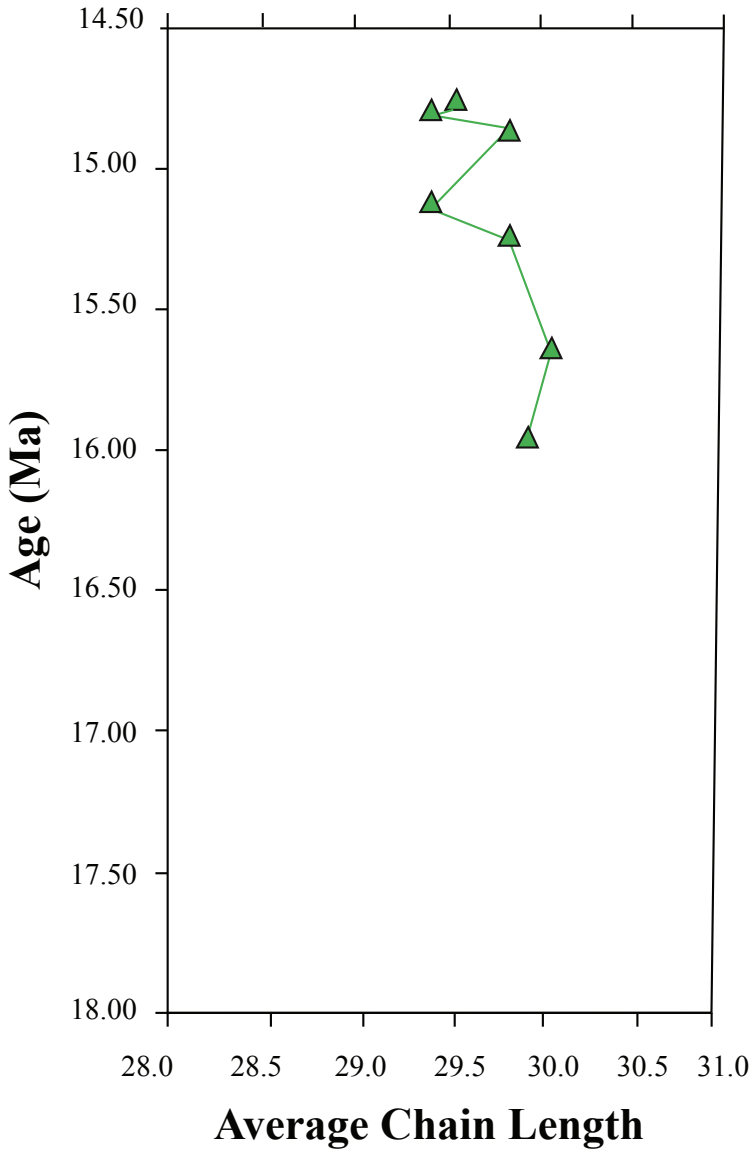

Fig. 11: Average chain length of *n*-alkanes extracted from sediments deposited in Hepburn's Mesa.

δD Composition of n-alkanes

The δD composition of C_{27}, C_{29}, and C_{31} *n*-alkanes from Railroad Canyon are positively correlated, indicating analogous plant sourcing. Weighted averages of δD and peak areas were

calculated in order to determine the average δD of the terrestrial plant community, yielding average δD values between -145‰ and -193‰ with an average of -175‰ (Figure 12). Between 17.5-17.35 Ma, *n*-alkane compositions increase by ~19‰ from a δD value of -178‰ to -157‰ and return to -183‰ by 16.56 Ma. A second increase of 44‰ occurs ~15.1 Ma and values return to -183‰ by 15 Ma. There is a 15‰ decrease in δD between the youngest and oldest samples in the section.

The δD composition of C_{29}, and C_{31} *n*-alkanes from Hepburn's Mesa are consistent with each other indicating analogous plant sourcing. C_{27} is invariant throughout the section, with an average δD of -194‰. Weighted averages of δD and peak areas yield average δD values of *n*-

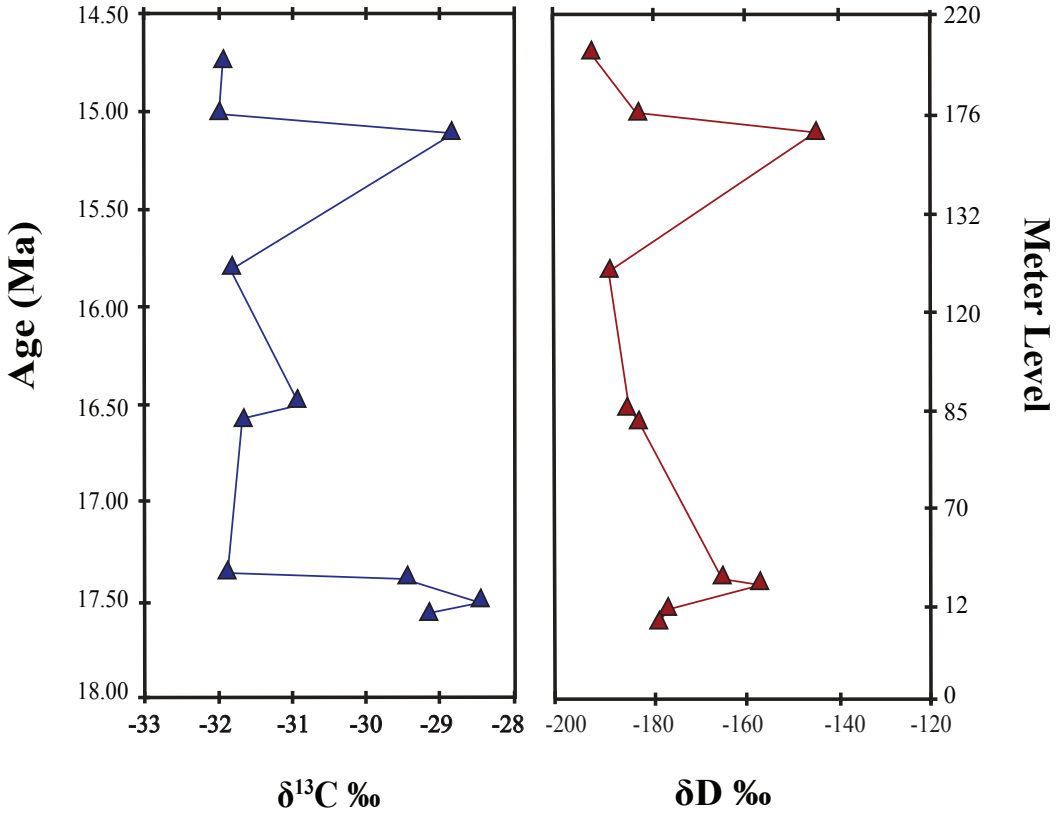

Fig. 12: Carbon and hydrogen isotopic composition of *n*-alkanes extracted from samples in Railroad Canyon.

alkanes for each sample varying between -179‰ and -197‰ with an average of -186‰ (Figure 13). At Hepburn's Mesa, the δD of samples increases by 20‰ between 15.7 and 15.3 Ma. By 14.9 Ma, δD values have returned to average. No broad shift in isotopic values is apparent throughout the section. The youngest value at Hepburn's Mesa is 6‰ heavier than the oldest value.

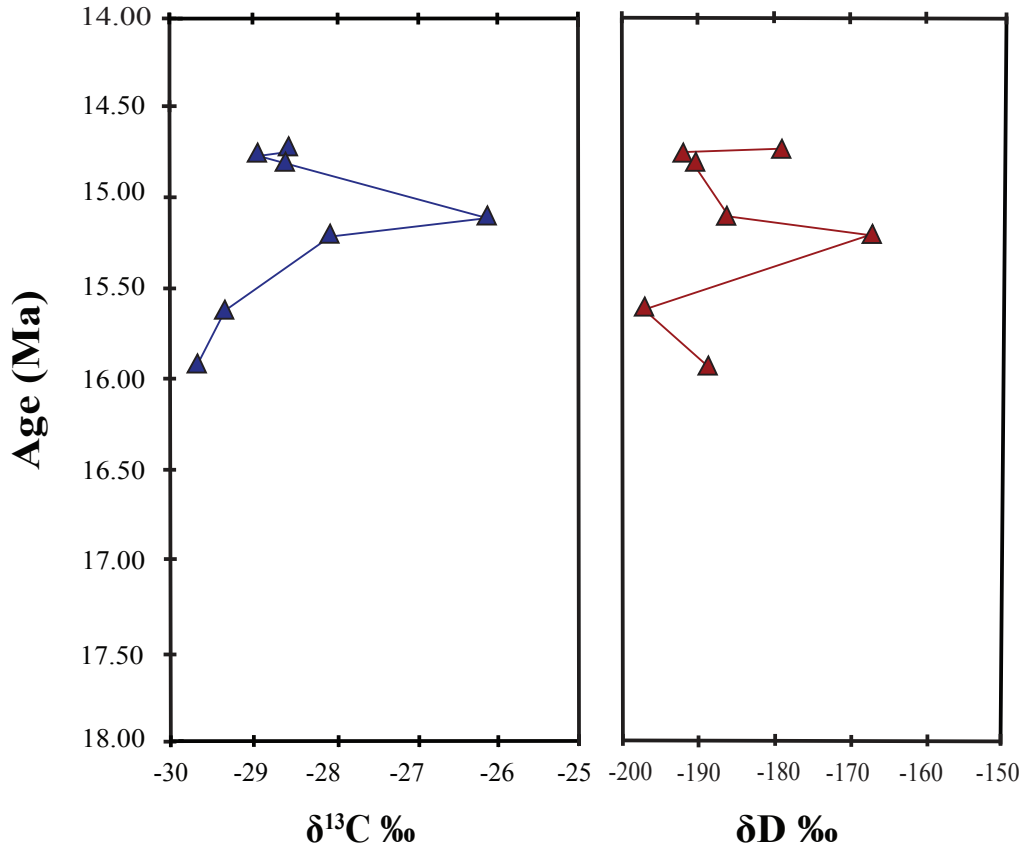

Fig. 13: Carbon and hydrogen isotopic composition of *n*-alkanes extracted from samples in Hepburn's Mesa.

$\delta^{13}C$ Composition of n-alkanes

The $\delta^{13}C$ values of C_{27}, C_{29}, and C_{31} from Railroad Canyon samples show similar trends throughout the section. Weighted averages of $\delta^{13}C$ and peak area for each sample yield average *n*-alkane $\delta^{13}C$ values varying between -28.4‰ and -31.9‰ with an average of -30.1‰ (Figure 12). Two increases in carbon isotopic composition can be observed in samples from the section. An increase of 1.7‰ from the mean occurs between 17.5-17.38 Ma, fully recovering by 17.35 Ma. Another increase of 3‰ occurs between 15.8-15.1 Ma. By 15.1 Ma $\delta^{13}C$ has returned to a lighter value of -32‰ and does not change throughout the rest of section.

The $\delta^{13}C$ values of C_{27}, C_{29}, and C_{31} from Hepburn's Mesa show similar trends throughout section. Weighted averages of $\delta^{13}C$ and peak area for each sample yield average *n*-alkane $\delta^{13}C$ values between -26.2‰ and -29.8‰ (Figure 13). Between 16.0 and 15.2 Ma the $\delta^{13}C$ of *n*-alkanes increases by 4.7‰. By 14.9 Ma $\delta^{13}C$ of *n*-alkanes decreases to 28.5‰ and does not change throughout the rest of section.

δD Composition of Volcanic Glasses

The δD composition of volcanic glasses from Railroad Canyon vary between -107 and -134‰ with an average of -122‰ (Figure 14). Initially, δD increases by ~12‰ at 17.4 Ma before gradually decreasing by ~15‰ until 15.0 Ma. At 15.0 Ma, values sharply increase by ~22‰ and remain invariant through 14.91 Ma. Applying an equation empirically derived by Friedman et al. (1992) the δD composition of environmental water was calculated as follows:

The δD composition of environmental water parallels the δD composition of volcanic glasses. Values vary between -77 and -113‰ and the mean δD of environmental water is -93‰.

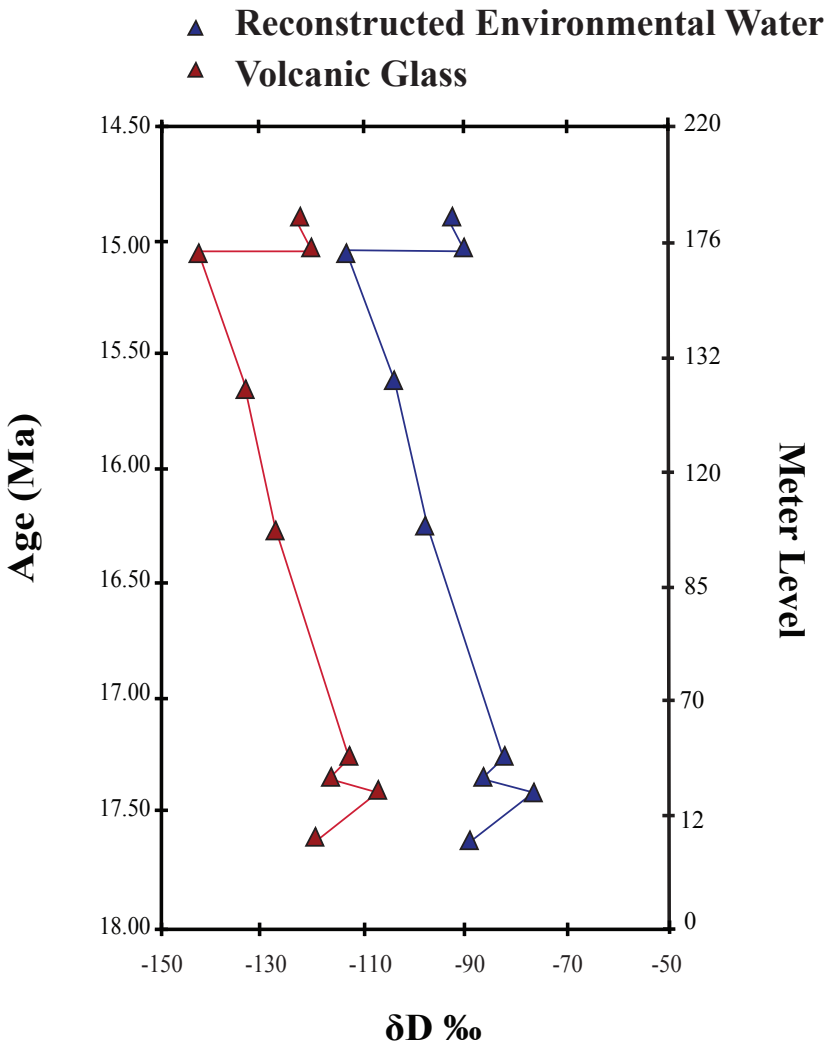

Fig. 14: Hydrogen isotopic composition of volcanic glasses (red) extracted from ashes deposited in Railroad Canyon and reconstructed precipitation (blue) for Railroad Canyon.

One ash was collected from the Hepburn's Mesa outcrop. It is from 14.61 Ma and has a δD composition of -135‰. Reconstructed environmental water from the ash is -105‰ and was calculated using the equation above.

Discussion

Compositional Integrity of n-alkanes

Modern studies have demonstrated that terrestrial plants synthesize *n*-alkanes between C_{23} and C_{35} with an odd over even chain-length predominance and that shorter ACL and smaller CPI values can be evidence of aquatic vegetation input or microbial degradation (Eglinton & Hamilton 1967; Huang et al. 1997; Zhou et al. 2010; Bianchi & Canuel 2011). ACL and CPI values calculated for both Railroad Canyon and Hepburn's Mesa are indicative of terrestrial plant sourcing with little degradation (Tables 1, 2). Additionally, samples collected from the Railroad Canyon basin preserve fossilized root traces suggesting that minimal diagenesis has occurred and that original isotopic compositions of *n*-alkanes remain intact (Schimmelman et al. 2006).

Climate Variability in Northwest U.S. during the Middle Miocene

Model simulations of climate incorporating Middle Miocene vegetation, topography, bathymetry, and modern pCO_2 suggest there was little summer change in effective moisture compared to modern and greater winter precipitation in the northwestern U.S. between 20 and 14

Ma (Herold et al. 2011). Molecular biomarkers of hydrology analyzed in this study reflect patterns in growing season hydrology and, similar to model results, describe arid basins akin to modern. Additionally, our results show that these regions experienced two periods of heightened aridity and fluctuations in source water composition during the Middle Miocene. Variability in the source and amount of precipitation suggests that the region experienced periods of climatic instability related to regional sourcing of warmer and

Table 1: Railroad Canyon n-alkanes distributions.

Meter Height	Age	$\delta D_{n\text{-alkanes}}$	δD_{C27}	δD_{C29}	δD_{C31}	$\delta^{13}C_{n\text{-alkanes}}$	$\delta^{13}C_{C27}$	$\delta^{13}C_{C29}$	$\delta^{13}C_{C31}$	ACL	CPI
210	14.70	-193	-190	-167	-196	-31.9	-31.1	-32.2	-32.0	28.3	3.1
175.6	15.00	-183	-174	-189	-199	-32.0	-32.8	-32.2	-31.5	29.1	4.0
157	15.10	-145	-127	-142	-133	-28.8	-29.3	-28.6	-28.5	28.2	1.4
137	15.80	-189	-177	-187	-211	-31.8	-32.4	-32.1	-30.6	28.4	3.7
85.1	16.49	-185	-175	-181	-159	-30.9	-30.6	-31.1	-30.9	28.3	3.3
79.4	16.56	-183	-177	-198	-174	-31.7	-31.5	-31.8	-31.7	28.2	2.6
79.6	16.90	-	-	-	-	-	-	-	-	29.4	3.0
36	17.35	-165	-191	-196	-153	-31.9	-32.3	-31.8	-31.8	29.31	4.3
34.8	17.37	-	-	-	-	-	-	-	-	28.6	1.6
34.3	17.38	-157	-157	-159	-151	-29.5	-29.1	-29.6	-29.7	28.5	1.4
32	17.40	-	-	-	-	-	-	-	-	28.8	3.0
30	17.43	-	-	-	-	-	-	-	-	28.2	1.2
11.9	17.50	-176	-167	-175	-169	-28.4	-28.4	-28.6	-28.3	28.2	2.4
5.9	17.56	-178	-169	-173	-177	-29.1	-28.0	-29.3	-30.0	28.5	4.5

Table 2: Hepburn's Mesa *n*-alkane distributions.

Meter Height	Age	$\delta D_{n\text{-alkanes}}$	δD_{C27}	δD_{C29}	δD_{C31}	$\delta^{13}C_{n\text{-alkanes}}$	$\delta^{13}C_{C27}$	$\delta^{13}C_{C29}$	$\delta^{13}C_{C31}$	ACL	CPI
52.0	14.79	-179.2	-192.7	-191.5	-169.5	-28.7	-28.3	-28.6	-28.8	29.5	6.6
51.0	14.81	-192.1	-176.4	-193.1	-195.8	-29.0	-28.6	-28.7	-29.4	29.4	6.4
48.0	14.86	-190.8	-193.2	-191.0	-183.0	-28.5	-28.6	-28.2	-28.8	29.8	6.5
41.0	15.15	-185.9	-205.2	-196.8	-168.6	-26.2	-27.6	-26.5	-25.8	29.4	4.5
39.5	15.25	-167.4	-201.4	-163.1	-168.6	-28.1	-28.0	-27.4	-28.7	29.9	8.1
27.0	15.66	-197.1	-204.8	-193.5	-196.5	-29.4	-28.7	-29.0	-30.0	30.1	6.9
18.0	15.96	-188.8	-187.1	-195.3	-183.4	-29.8	-28.6	-29.4	-30.5	29.9	15.8

enriched subtropical water.

Volcanic glasses provide estimates of the isotopic composition of plant source water prior to fractionation during plant water uptake (Friedman et al. 1992; Mulch et al. 2008; Cassel et al. 2009; Dettinger 2013). Depending on the environment and the plant taxa, the primary water source may be summer rainfall, winter snow melt, stream water, or subsurface water (Welker 2000). Hou et al. (2008) demonstrated that in regions with low annual rainfall, precipitation is the greatest water source for leaf wax biosynthesis. Biostratigraphic and lithostratigraphic studies suggest that Railroad Canyon and Hepburn's Mesa sediments were deposited in arid basins during the Middle Miocene, indicating that precipitation was the primary water source for plants living in this region 18-14 Ma (Barnosky & Labar 1989; Barnosky et al. 2007; Hou et al. 2008). The δD of precipitation can be used with the δD of *n*-alkanes to calculate the apparent fractionation ($\varepsilon_{apparent}$), which is a measure of the moisture content of an ecosystem, using the following equation:

$$\varepsilon_{apparent} = 1000 * \left[\frac{\delta D_{n-alkane} + 1000}{\delta D_{precipitation} + 1000} - 1 \right]$$

$\varepsilon_{apparent}$ measures the isotopic difference between source water and the subsequent waxes produced by plants and is affected by evapotranspiration processes of the soil and leaf water of the plant. Using the average δD of reconstructed environmental water and the average δD of leaf waxes, $\varepsilon_{apparent}$ of Railroad Canyon and Hepburn's Mesa was determined to be -92.4‰ and -90.3‰, respectively. These values are similar to $\varepsilon_{apparent}$ of modern arid environments and agree with prior studies based upon biostratigraphic and lithostratigraphic analyses of both basins

(Barnosky & Labar 1989; Barnosky et al. 2007; Feakins & Sessions 2010; Polissar & Freeman 2010).

Estimated δD of precipitation from volcanic ashes deposited in the Railroad Canyon and Hepburn's Mesa basins are similar to modern values of ~100‰ (Table 3) (Bowen and Revenaugh 2003). The two intervals of enriched precipitation in the Railroad Canyon basin that occurr at ~17.3 and ~15.0 Ma can be attributed to changes in the source of water masses producing rainfall in the region that integrated enriched subtropical water (Figure 14). Shifts in precipitation are contemporaneous with enriched δD values of *n*-alkanes in both basins and indicate subtropical water sourcing contributed to the enrichment of terrestrial leaf waxes as well (Figures 12, 13). However, the magnitude of *n*-alkane enrichment in both instances is greater than the shift in precipitation observed from volcanic glasses. Higher rates of evaporation from soil water and transpiration of leaf water during leaf wax synthesis would enhance δD

Table 3: Measured volcanic glass and calculated precipitation isotopic distributions.

Meter Height	Age	δD Glass	δD Precipitation
176	14.91	-123.2	-93.1
172.8	15.02	-120.6	-90.4
171.1	15.03	-142.85	-113.4
134.2	15.59	-134.2	-104.5
127.9	16.23	-127.7	-97.8
52.5	17.24	-113.15	-82.7
37.5	17.33	-117.35	-87.1
30	17.39	-107.55	-76.9
0	17.60	-119.5	-89.3

enrichment and suggests that changes to precipitation source water was accompanied by hydrologic changes promoting drier conditions in inland basins during the Middle Miocene.

$\delta^{13}C$ records of leaf waxes from the basins are consistent with heightened aridity affecting the basins at ~17.3 and ~15.0 Ma. Aside from these periods of enrichment, the $\delta^{13}C$ of samples from Railroad Canyon is stable at ~32‰. Enriched $\delta^{13}C$ values of *n*-alkanes suggest plants altered stomata regulation in order to minimize transpiration during these intervals of increased water stress. In other words, $\delta^{13}C$ data corroborate the physical fractionation signal from δD data of volcanic glass and leaf waxes through an independent biologic process (Figures 12, 13). Furthermore, previous studies have determined the $\delta^{18}O$ of pedogenic carbonates from Railroad Canyon. Affected by similar processes as δD of soil water, lighter oxygen is evaporated from soil water in arid landscapes before being incorporated into terrestrial carbonates. Enriched $\delta^{18}O$ values of pedogenic carbonates are found in the Railroad Canyon basin at ages similar to those of the δD and $\delta^{13}C$ of leaf waxes, also demonstrating episodic pulses of aridity affected the region during the Middle Miocene (Figure 15) (Kent-Corson et al. 2006). Altogether, these temporally similar fluctuations in source water composition and evapotranspiration rates imply recurrent disruptions to ambient climate patterns when lower latitude water provided moisture to the northwestern U.S. and drier conditions persisted in inland basins.

Miocene fossil distributions from the northern coast of North America provide evidence for a subtropical pool of warm water intermittently present in the north Pacific. Oleinik et al. (2008) examined bivalves deposited within Middle Miocene sedimentary beds in Kodiak Island, Alaska, and the Kamchatka Peninsula in order to determine the magnitude of warming at high

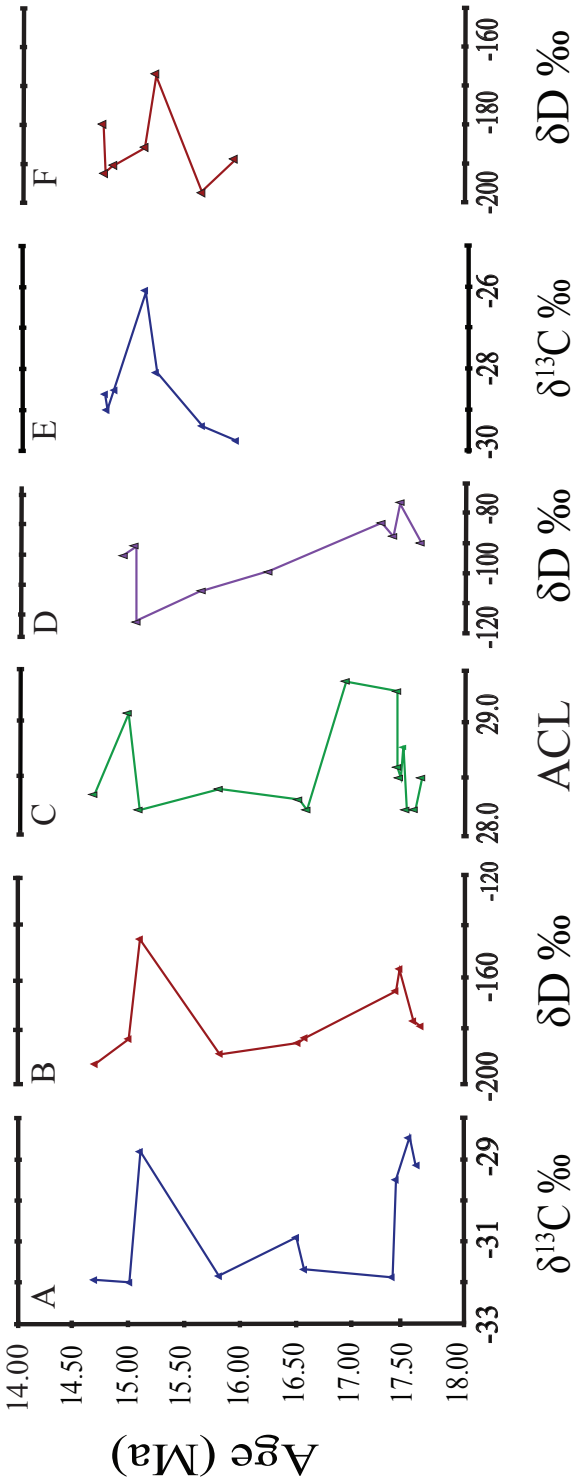

Fig. 15: Carbon and hydrogen isotopic compositions of *n*-alkanes extracted from samples collected from Railroad Canyon (A,B), ACL of *n*-alkanes from Railroad Canyon (C), hydrogen isotopic composition of volcanic glasses from Railroad Canyon (D), carbon and hydrogen isotopic compositions of *n*-alkanes from Hepburn's Mesa (E,F) with age.

latitude environments. They found dominantly cool-water mollusks epidsodically replaced by beds of warm-water mollusks when north Pacific surface water MAT reached 23.5 ºC. The intermittent distribution of warm-water mollusks in the north Pacific implies a Middle Miocene climate pattern that did not manifest as a single warming event but as several cool and warm episodes facilitated by the incursion and retreat of warm, sub-equatorial Pacific water into the North Pacific (Oleinik et al. 2008). The presence of a subtropical water mass off of the coast of North America provides a potential source for the enriched precipitation observed from ashes deposited in the Railroad Canyon basin during the Middle Miocene at ~17.4 and ~15.0 Ma. This scenario argues for a dynamic climate in northwestern North America during the Middle Miocene tied to the movement and distribution of warm equatorial water.

In the modern, the Pacific/North American teleconnection pattern (PNAS) strongly influences surface climate in the mid-latitudes of the northern hemisphere. The PNAS is a climate pattern consisting of high and low pressure systems that affects weather delivered by the East Asian jet stream to North America and accounts for most climate variability observed throughout much of North America, including the modern Railroad Canyon and Hepburn's Mesa locations (Leathers et al. 1991). During positive phases, a high pressure system resides over western North America, typically delivering less precipitation and warmer weather to the region. During negative phases the opposite occurs, with cooler and wetter weather dominating the area (Leathers et al. 1991). The PNAS is anchored by the positioning of the Cordillera and Tibetan Plateau as well as the land-sea temperature differences between the Pacific Ocean and East Asia/ Western North America continents (Leathers & Palecki 1992). As both the Cordillera and the Tibetan Plateau were in place by the Middle Miocene, it is likely that the PNAS affected the

climate of Railroad Canyon and Hepburn's Mesa basins during the time of leaf wax deposition just as it does now (Horton et al. 2004; Graham et al. 2005; Kent-Corson et al. 2006; Rowley & Currie 2006).

Terrestrial Plant Composition and Input at Railroad Canyon and Hepburn's Mesa

ACL increases at ~17.4 and ~15.0 Ma, mirroring δD and $\delta^{13}C$ patterns of leaf waxes and further demonstrating plant responses to episodes of warmth and aridity in the Railroad Canyon community during the Middle Miocene. Disparity in the ACL and $\delta^{13}C$ values of samples collected from Hepburn's Mesa and Railroad Canyon suggests that Hepburn's Mesa received greater C_4 plant contribution during the Middle Miocene. While C_3 plants dominated arid grasslands throughout the Miocene until ~5 Ma, phytolith evidence for the presence of C_4 plants in the northwestern U.S. exists as early as 19 Ma (Tipple & Pagani 2010; Strömberg & McInerney 2011). Samples from Hepburn's Mesa contain longer-chain *n*-alkanes and show less variation in chain length through section than samples collected from Railroad Canyon. Additionally, the $\delta^{13}C$ of *n*-alkanes from Hepburn's Mesa are isotopically heavier than those from Railroad Canyon, another characteristic of C_4 vegetation. Both ancient ecosystems were dominated by C_3 vegetation; however, ACL and $\delta^{13}C$ indicate greater C_4 plant abundance at the Hepburn's Mesa basin and supports the presence of C_4 plants in C_3 dominated grasslands prior to C_4 plant expansion during the late Miocene (Farquhar 1989; Strömberg 2005; Tipple & Pagani 2010).

Conclusion

This study examined the δD and $\delta^{13}C$ of leaf waxes and volcanic glasses extracted from lithified mudstones and siltstones deposited within intermontane basins in southwestern Montana. Railroad Canyon and Hepburn's Mesa basins received sediments during the Middle Miocene climatic optimum, a warm interval set within a long-term trend of Cenozoic cooling during which global temperatures were 3-6ºC warmer than present and pCO_2 was 450-600 ppm. δD of volcanic glasses revealed slightly more enriched precipitation during the Miocene than the modern at Railroad Canyon and similar δD of precipitation to the modern at Hepburn's Mesa. $\varepsilon_{apparent}$ showed similar to modern evapotranspiration rates for both basins, indicating that aridity is a persistent feature of intermontane basins in southwestern Montana. Extracted *n*-alkanes from Railroad Canyon show two periods of synchronous δD and $\delta^{13}C$ enrichment at ~17.3 and ~15.0 Ma. Samples from Hepburn's Mesa also showed enrichment in both δD and $\delta^{13}C$ at 15.0 Ma. Concurrent with δD and $\delta^{13}C$ enrichment, we observed elongation of the average chain length of *n*-alkanes from Railroad Canyon. These data suggest two intervals of heightened aridity struck Railroad Canyon and Hepburn's Mesa at ~17.3 and ~15.0 Ma, but these episodes were short-lived.

Future climate projections disagree upon whether precipitation will increase or decrease in these basins as global temperature increases over the next century (Solomon et al. 2009). Analyses of molecular biomarkers from the Middle Miocene ecosystem describe a drier climate with episodes of heightened aridity. These swings in precipitation may have been driven by intermittent movement of warm, equatorial Pacific water into the Nothern Pacific during a time

of increased temperature and pCO_2. At the Railroad Canyon and Hepburn's Mesa localities modern variation in temperature and precipitation is driven by modal changes of the Pacific-North American teleconnection system. As this climate pattern is governed in part by temperature gradients between ocean and land surfaces, how it is affected by increased global air temperature should be a focus for climate projections for that region.

Appendix

XRD traces of volcanic glasses examined in this study.

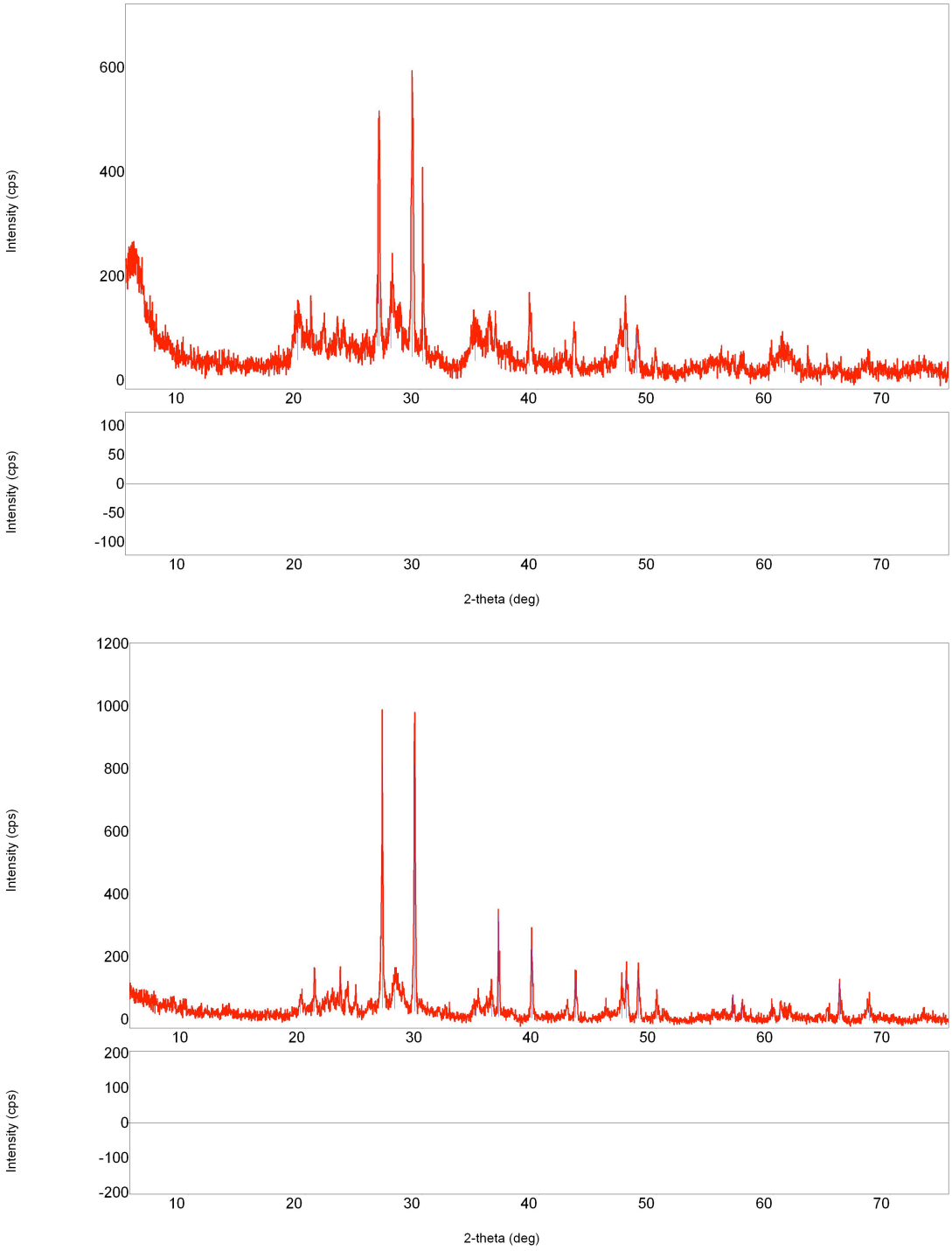

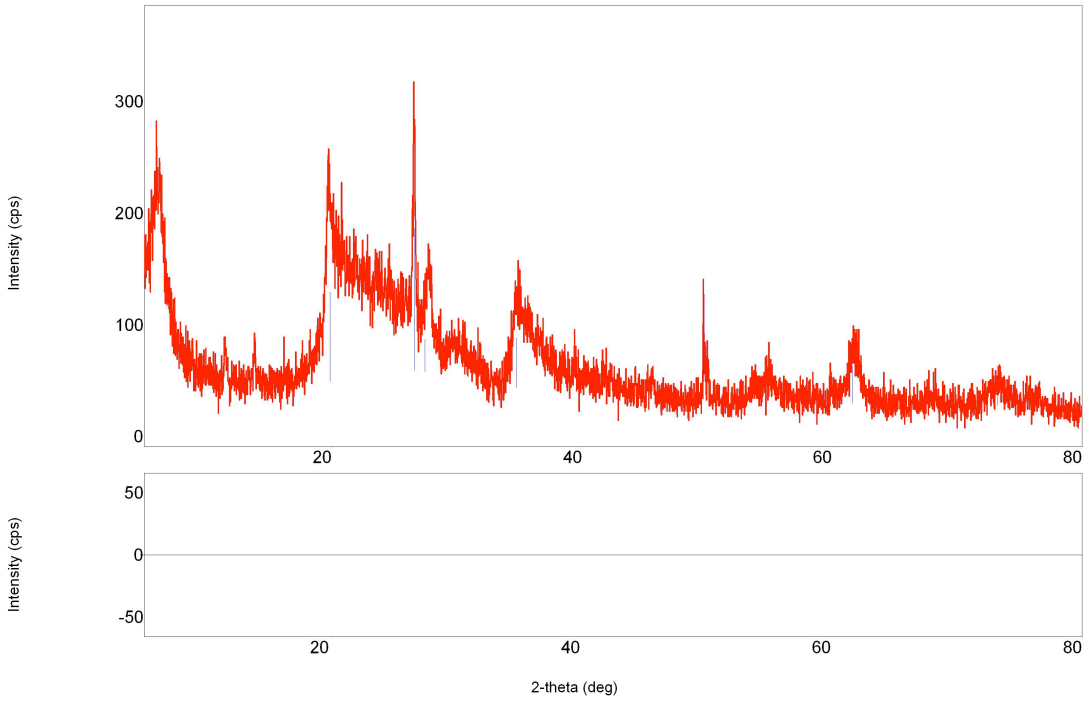
Intensity (cps)
300
200
100
0
20
40
60
80
Intensity (cps)
50
0
-50
20
40
60
80
2-theta (deg)

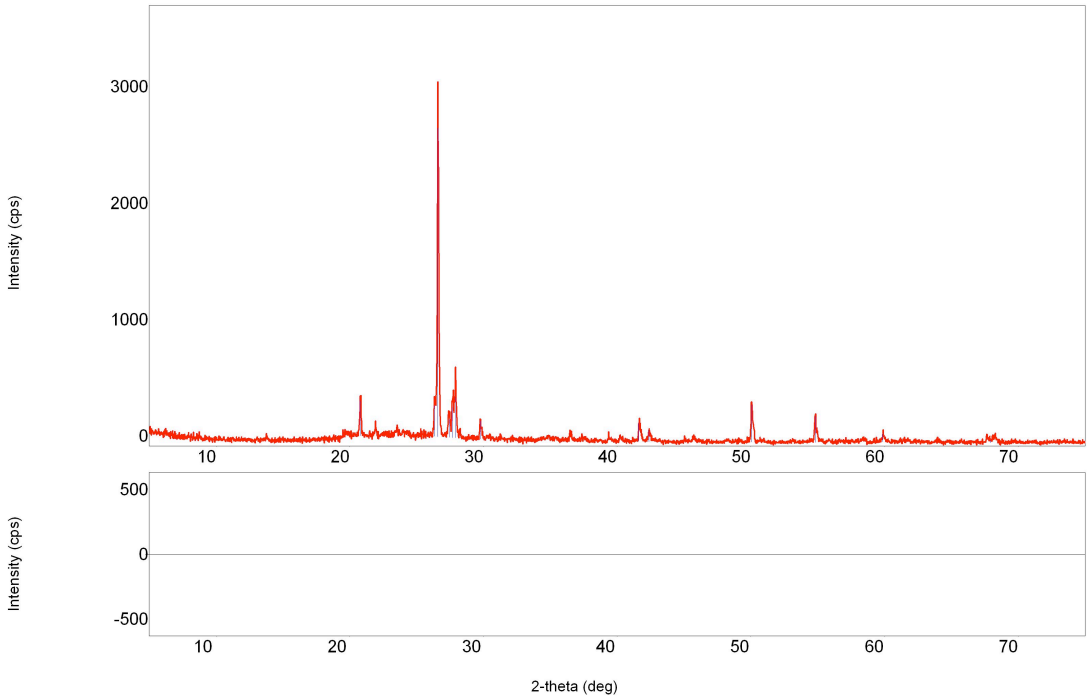
Intensity (cps)
3000
2000
1000
0
10
20
30
40
50
60
70
Intensity (cps)
500
0
-500
10
20
30
40
50
60
70
2-theta (deg)

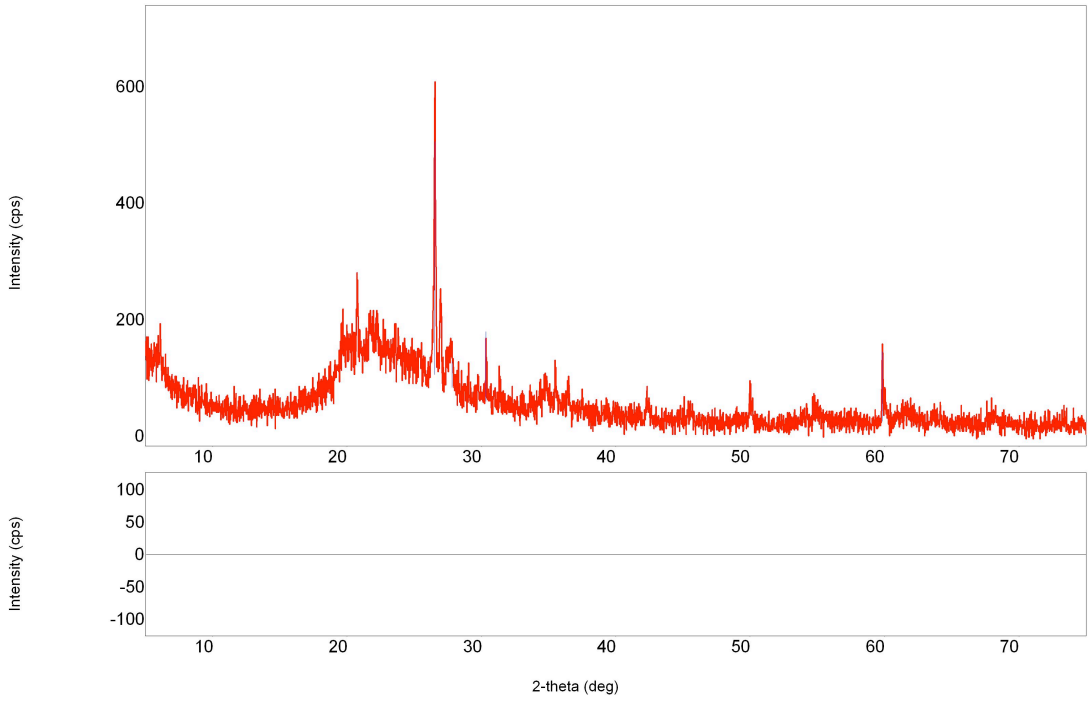
Intensity (cps)
600
400
200
0
10
20
30
40
50
60
70
Intensity (cps)
100
50
0
-50
-100
10
20
30
40
50
60
70
2-theta (deg)

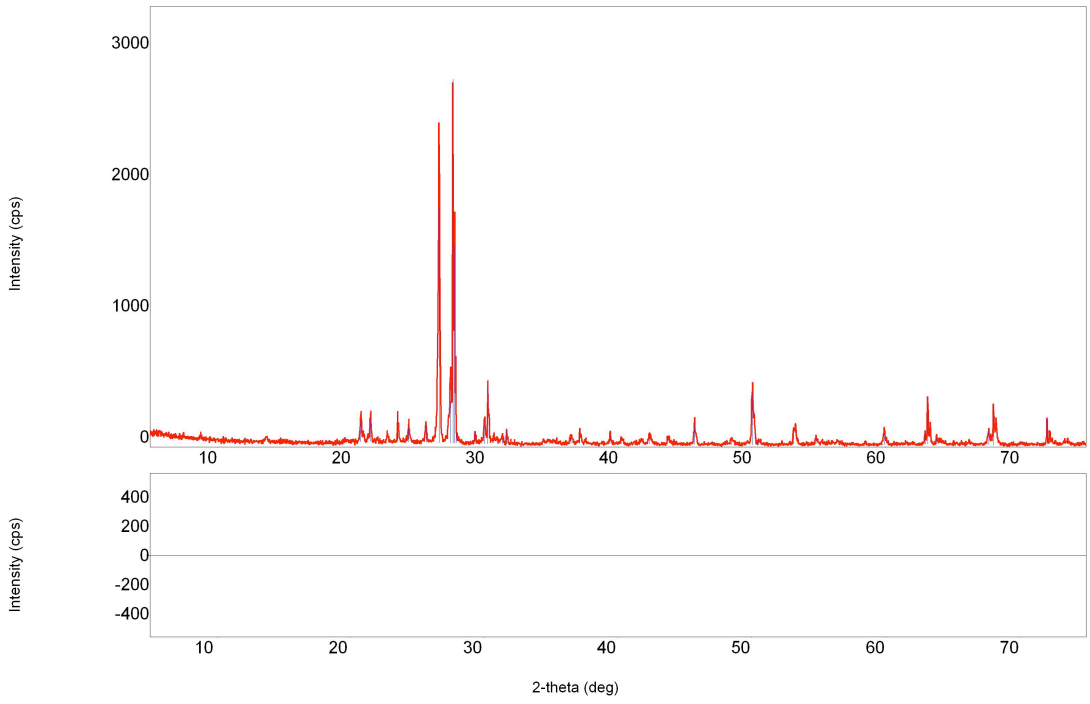
Intensity (cps)
3000
2000
1000
0
10
20
30
40
50
60
70
Intensity (cps)
400
200
0
-200
-400
10
20
30
40
50
60
70
2-theta (deg)

Isotopic composition of *n*-alkanes.

	$\delta^{13}C\ C_{27}$	$\delta^{13}C\ C_{29}$	$\delta^{13}C\ C_{31}$	$\delta D\ C_{27}$	$\delta D\ C_{27}$	$\delta D\ C_{27}$
MT-09-RR-14	-29.67737484	-28.83685325	-28.59700929	-109	-147	-149
	-28.85862335	-28.46168025	-28.38483804	-146	-138	-116
MT-09-RR-2	-28.4057928	-28.55490438	-28.29024587	-176	-183	-174
				-159	-166	-164
MT-14-RR-7F	-31.49380056	-32.4671662	-31.79360915	-190	-167	-196
	-30.76197818	-32.02934541	-32.2014346			
MT-14-RR-4A	-33.80896284	-32.04717748	-31.91626561	-191	-196	-153
	-30.74335284	-31.51733023	-31.606368			
MT-09-RR-7	-29.18124282	-29.61076576	-29.7361781	-157	-159	-151
	-29.03452171	-29.63110143	-29.61143307			
MT-14-HM-7	-28.33286493	-28.56327244	-28.7762724	-193	-192	-169
	-28.23738651	-28.71244896	-28.8860219			
MT-14-HM-5	-28.40386518	-28.29490002	-28.75509653	-193	-191	-183
	-28.74931264	-28.1907654	-28.86030079			
MT-14-HM-4	-27.53223535	-26.51660161	-25.7949702	-205	-197	-169
	-27.57479247	-26.54755807	-25.7888091			
MT-14-HM-1	-28.65577426	-29.38000763	-30.37031443	-187	-195	-183
	-28.49312027	-29.35968289	-30.55787078			
MT-14-HM-9	-28.75608887	-28.89362412	-29.12355141	-176	-193	-196
	-28.4921856	-28.58816602	-29.6563364			
MT-14-HM-3	-27.99210923	-27.51374107	-28.82998381	-201	-163	-169
	-27.9092958	-27.35425859	-28.61881853			
MT-14-HM-2	-28.62119433	-29.0600744	-30.05139998	-205	-193	-197
	-28.85338215	-28.86626072	-29.93750881			
MT-14-RR-5E	-31.91042696	-32.91166095	-32.30043048	-177	-187	-211
	-30.1248576	-32.31000221	-31.16188307			
MT-14-RR-6D	-32.44620756	-32.07060317	-30.62476616	-174	-189	-199
	-33.16002295	-32.39155529	-32.41581592			
MT-14-RR-5A	-30.61621872	-31.06071823	-30.79864039	-175	-181	-159
	-30.5911405	-31.11553996	-30.96161773			
MT-14-RR-4K	-31.51450081	-31.79711503	-31.76005828	-177	-198	-174
	-31.53402346	-31.80031486	-31.60706372			
MT-09-RR-1	-27.96467233	-29.25197717	-29.96734532	-179	-180	-184
				-159	-165	-170

Isotopic Composition of volcanic glasses.

	δD
MT-14-RR-7A	-119.5
	-126.9
MT-14-RR-6C	-123.7
	-117.5
MT-14-RR-6B	-141.7
	-144.0
MT-14-RR-5D	-136.5
	-131.9
MT-14-RR-5C	-130.1
	-125.3
MT-14-RR-4F	-113.0
	-113.3
MT-14-RR-4B	-113.7
	-121.0
MT-14-RR-3A	-109.1
	-106.0
MT-14-RR-1A	-121.9
	-117.1

Works Cited

Barnosky, A. D., Bibi, F., Hopkins, S. S., & Nichols, R., 2007, Biostratigraphy and magnetostratigraphy of the mid-Miocene Railroad Canyon Sequence, Montana and Idaho, and age of the mid-Tertiary unconformity west of the continental divide: *Journal of Vertebrate Paleontology*, v. 27, p. 204-224.

Barnosky, A. D. & Labar, W. J, 1989, Mid-Miocene (Barstovian) environmental and tectonic setting near Yellowstone Park, Wyoming and Montana: *Geological Society of America Bulletin*, v. 101, p. 1448-1456.

Bianchi, T. & Canuel, E., 2011, Chemical Biomarkers in Aquatic Ecosystems: Princeton, Princeton University Press, 392 p.

Bonal, D., Sabatier, D., Montpied, P., Tremeaux, D., & Guehl, J. M., 2000, Interspecific variability of δ13C among trees in rainforests of French Guiana: functional groups and canopy integration: *Oecologia*, v. 124, p. 454-468.

Bowen, G. J. & Revenaugh, J., 2003, Interpolating the isotopic composition of modern meteoric precipitation: *Water Resources Research*, v. 39, p. 1-13.

Brocks, J. & Pearson, A., 2005, Building the biomarker tree of life: *Reviews in Mineralogy & Geochemistry*, v. 59, p. 233-258.

Bush, R. T. & McInerney, F. A., 2013, Leaf wax *n*-alkane distributions in and across modern plants: Implications for paleoecology and chemotaxonomy: *Geochimica et Cosmochimica Acta*, v. 117, p. 161-179.

Cassel, E. J., Graham, S. A., & Chamberlain, C. P., 2009, Cenozoic tectonic and topographic evolution of the northern Sierra Nevada, California, through stable isotope paleoaltimetry in volcanic glass: *Geology*, v. 37, p. 547-550.

Cassel, E. J., Graham, S. A., Chamberlain, C. P., & Henry, C. D., 2012, Early Cenozoic topography, morphology, and tectonics of the northern Sierra Nevada and western Basin and Range: *Geosphere*, v. 8, p. 229-249.

Castañeda, I. S., Werne, J. P., & Johnson, T. C., 2007, Wet and arid phases in the southeast African tropics since the Last Glacial Maximum: *Geology*, v. 35, p. 823-826.

Castañeda, I. S., Mulitza, S., Schefuß, E., dos Santos, R. A. L., Damsté, J. S. S., & Schouten, S., 2009, Wet phases in the Sahara/Sahel region and human migration patterns in North Africa: *Proceedings of the National Academy of Sciences*. v. 106, p. 20159-20163.

Cerling, T. E., Harris, J. M., MacFadden, B. J., Leakey, M. G., Quade, J., Eisenmann, V., & Ehleringer, J., 1997, Global vegetation change through the Miocene and Pliocene: *Nature*, v. 389, p. 153-158.

Chamberlain, C. P. & Poage, M. A., 2000, Reconstructing the paleotopography of mountain belts from the isotopic composition of authigenic minerals: *Geology,* v. 28, p. 115-118.

Chikaraishi, Y. & Naraoka, H., 2003, Compound-specific δD-$\delta^{13}C$ analyses of *n*-alkanes extracted from terrestrial and aquatic plants: *Phytochemistry*, v. 63, p. 361-371.

Coney, P. J., & Harms, T. A., 1984, Cordilleran metamorphic core complexes: Cenozoic extensional relics of Mesozoic compression: *Geology*, v. 12, p. 550-554.

Coney, P. J., 1987, The regional tectonic setting and possible causes of Cenozoic extension in the North American Cordillera: *Geological Society, London, Special Publications*, v. 28, p. 177-186.

Craig, H., 1954, Geochemical implications of the isotopic composition of carbon in ancient rocks: *Geochimicha et Cosmochimica Acta,* v. 6, p. 186-196.

Dansgaard, W., 1964, Stable isotopes in precipitation: *Tellus A*, v. 16, p. 436-468.

Dettinger, M. P., 2013, Calibrating and testing the volcanic glass paleoaltimeter in South America. [Ph.D thesis]: University of Arizona, 38 p.

Eglinton, G. & Hamilton, R.J., 1967, Leaf epiticular waxes: *Science*, v. 156, p. 1322-1335.

Farquhar, G. D. & Sharkey, T. D., 1982, Stomatal conductance and photosynthesis: *Annual Reviews Plant Physiology*, v. 33, p. 317-345.

Farquhar, G. D., O'Leary, M. H., & Berry, J. A., 1982, On the relationship between carbon isotope discrimination and the intercellular carbon dioxide concentration in leaves: *Australian Journal of Plant Physiology*, v. 9, p. 121-137.

Farquhar, G. D., 1989, Models of integrated photosynthesis of cells and leaves: *Philosophical Transactions of the Royal Society B: Biological Sciences*, v. 323, p. 357-367.

Feakins, S. J. & Sessions, A. L., 2010, Controls on the D/H ratios of plant leaf waxes in an arid ecosystem: *Geochimica et Cosmochimica Acta*, v. 74, p. 2128-2141.

Feakins, S. J., Levin, N. E., Liddy, H. M., Sieracki, A., Eglinton, T. I., & Bonnefille, R., 2013, Northeast African vegetation change over 12 my: *Geology*, v. 41, p. 295-298.

Feakins, S. J., Warny, S., & Lee, J. E., 2012, Hydrologic cycling over Antarctica during the middle Miocene warming: *Nature Geoscience*, v. 5, p. 557-560.

Flanagan, L. B., Bain, J. F., & Ehleringer, J. R., 1991, Stable oxygen and hydrogen isotope composition of leaf water in C3 and C4 plant species under field conditions: *Oecologia*, v. 88, p. 394-400.

Flowers, B. P. & Kennett, J. P., 1994, The middle Miocene climatic transition: East Antarctic ice sheet development, deep ocean circulation and global carbon cycling: *Palaeogeography, Palaeoclimatology, Palaeoecology*, v. 108, p. 537-555.

Foster, G. L., Lear, C. H., & Rae, J. W., 2012, The evolution of pCO_2, ice volume and climate during the middle Miocene: *Earth and Planetary Science Letters*, v. 341, p. 243-254.

Fox, D. L. & Koch, P. L., 2003, Tertiary history of C_4 biomass in the Great Plains, USA: *Geology,* v. 31, p. 809-812.

Fox, D. L. & Koch, P. L. 2004. Carbon and oxygen isotopic variability in Neogene paleosol carbonates: constraints on the evolution of the C_4-grasslands of the Great Plains, USA. *Palaeogeography, Palaeoclimatology, Palaeoecology*, v. 207, p. 305-329.

Friedman I, Sheppard RA, & Gude AJ., 1993, Deuterium Fractionation as water diffuses into silicic volcanic ash *in* Swart, P. K., Lohmann, K. C., Mckenzie, J., & Savin, S. eds, Climate Change in Continental Isotopic Records: Washington, D.C., American Geophysical Union, p. 321–323.

Gagosian, R. B., & Peltzer, E. T., 1986, The importance of atmospheric input of terrestrial organic material to deep sea sediments: *Organic Geochemistry*, v. 10, p. 661-669.

Gat, J. R., 1996, Oxygen and hydrogen isotopes in the hydrologic cycle: *Annual Reviews Earth Planetary Science*, v. 24, p. 225-62.

Goudriaan, J. & van Laar, H., 1978, Relations between leaf resistance, *CO* concentration and assimilation in maize, beans, grass and sunflower: *Photosynthetica,* v. 12, p. 241-249.

Graham, S. A., Chamberlain, C. P., Yue, Y., Ritts, B. D., Hanson, A. D., Horton, T. W., Waldbauer J.R., Poage M.A., & Feng X., 2005, Stable isotope records of Cenozoic climate and topography, Tibetan plateau and Tarim basin: *American Journal of Science*, v. 305, p. 101-118.

Hodell, D. A. & Woodruff, F., 1994, Variations in the strontium isotopic ratio of seawater during the Miocene: Stratigraphic and geochemical implications: *Paleoceanography*, v. 9, p. 405-426.

Holbourn, A., Kuhnt, W., Schulz, M., Flores, J. A., & Andersen, N., 2007, Orbitally-paced climate evolution during the middle Miocene "Monterey" carbon-isotope excursion: *Earth and Planetary Science Letters*, v. 261, p. 534-550.

Holbourn, A., Kuhnt, W., Frank, M., & Haley, B. A., 2013, Changes in Pacific Ocean circulation following the Miocene onset of permanent Antarctic ice cover: *Earth and Planetary Science Letters*, v. 365, p. 38-50.

Horton, T., Sjostrom, D., Abruzzese, M., Poage, M., Waldbauer, J., Hren, M., Wooden, J., & Chamberlain, C. P., 2004, Spatial and temporal variation of Cenozoic surface elevation in the Great Basin and Sierra Nevada: *American Journal of Science*, v. 304, p. 862-888.

Hou, J., D'Andrea, W. J., MacDonald, D., & Huang, Y., 2007, Hydrogen isotopic variability in leaf waxes among terrestrial and aquatic plants around Blood Pond, Massachusetts, USA: *Organic Geochemistry*, v. 38, p. 977-984.

Hou, J., D'Andrea, W. J., & Huang, Y., 2008, Can sedimentary leaf waxes record D/H ratios of continental precipitation? Field, model, and experimental assessments: *Geochimica et Coscmochimica Acta*, v. 72, p. 3503-3517.

Huang, Y., Eglinton, G., Ineson, P., Latter, P. M., Bol, R., & Harkness, D. D., 1997, Absence of carbon isotope fractionation of individual n-alkanes in a 23-year field decomposition experiment with *Calluna vulgaris*: *Organic Geochemistry*, v. 26, p. 497-501.

Hughen, K. A., Eglinton, T. I., Xu, L., & Makou, M., 2004, Abrupt tropical vegetation response to rapid climate changes: *Science*, v. 304, p. 1955-1959.

Kennett, J. P., 1977, Cenozoic evolution of Antarctic glaciation, the circum−Antarctic Ocean, and their impact on global paleoceanography: *Journal of Geophysical Research*, v. 82, p. 3843-3860.

Kent-Corson, M. L., Sherman, L. S., Mulch, A., & Chamberlain, C. P., 2006, Cenozoic topographic and climatic response to changing tectonic boundary conditions in Western North America: *Earth and Planetary Science Letters*, v. 252, p. 453-466.

Kunst, L. & Samuels, A. L., 2003, Biosynthesis and secretion of plant cuticular wax: *Lipid Research*, v. 42, p. 51-80.

Kürschner, W. M., Kvaček, Z., & Dilcher, D. L., 2008, The impact of Miocene atmospheric carbon dioxide fluctuations on climate and the evolution of terrestrial ecosystems: *Proceedings of the National Academy of Sciences*, v. 105, p. 449-453.

Lauteri, M., Scartazza, A., Guido, M. C., & Brugnoli, E., 1997, Genetic variation in photosynthetic capacity, carbon isotope discrimination and mesophyll conductance in

provenances of *Castanea sativa* adapted to different environments: *Functional ecology*, v. 11, p. 675-683.

Leathers, D. J., Yarnal, B., & Palecki, M. A., 1991, The Pacific/North American teleconnection pattern and United States climate. Part I: Regional temperature and precipitation associations: *Journal of Climate*, v. 4, p. 517-528.

Leathers, D. J. & Palecki, M. A., 1992, The Pacific/North American teleconnection pattern and United States climate. Part II: temporal characteristics and index specification: *Journal of Climate*, v. 5, p. 707-716.

Liu, W. & Huang, Y., 2005, Compound specific D/H ratios and molecular distributions of higher plant leaf waxes as novel paleoenvironmental indicators in the Chinese Loess Plateau: *Organic Geochemistry*, v. 36, p. 851-860.

Liu, W., & Yang, H., 2008, Multiple controls for the variability of hydrogen isotopic compositions in higher plant n-alkanes from modern ecosystems: *Global Change Biology*, v. 14, p. 2166-2177.

Miller, E. L., & Gans, P. B., 1989, Cretaceous crustal structure and metamorphism in the hinterland of the Sevier thrust belt, western US Cordillera: *Geology*, v. 17, p. 59-62.

Miller, K. G., Wright, J. D., & Fairbanks, R. G., 1991, Unlocking the ice house: Oligocene-Miocene oxygen isotopes, eustasy, and margin erosion: *Journal of Geophysical Research: Solid Earth (1978–2012)*, v. 96, p. 6829-6848.

Montagne, J., 1982a, Cenozoic structural history of the upper Yellowstone Valley, *in* Montagne, J., & Chadwick, R. A., eds., Cenozoic history of the Yellowstone Valley south of Livingston, Montana: Bozeman, Montana, Montana State University, p. 11-16.

Mulch, A., Sarna-Wojcicki, A. M., Perkins, M. E., & Chamberlain, C. P., 2008, A Miocene to Pleistocene climate and elevation record of the Sierra Nevada (California): *Proceedings of the National Academy of Sciences*, v. 105, p. 6819-6824.

Oleinik, A., Marincovich Jr, L., Barinov, K. B., & Swart, P. K., 2008, Magnitude of Middle Miocene warming in North Pacific high latitudes: Stable isotope evidence from *Kaneharaia* (Bivalvia, *Dosiniinae*): *Bulletin of the Geological Survey of Japan*, v. 59, p. 339-353.

Pagani, M., Freeman, K. H., & Arthur, M. A., 1999, Late Miocene atmospheric CO_2 concentrations and the expansion of C4 grasses: *Science*, v. 285, p. 876-879.

Pagani, M., Pedentchouk, N., Huber, M., Sluijs, A., Schouten, S., Brinkuis, H., Sinnighe Damste, J., & Dickens, G., 2006, Arctic hydrology during global warming at the Palaeocene/Eocene thermal maximum: *Nature,* v. 442, p. 671-675.

Panek, J. A., & Waring, R. H., 1997, Stable carbon isotopes as indicators of limitations to forest growth imposed by climate stress: *Ecological Applications*, v. 7, p. 854-863.

Passey, B. H., Cerling, T. E., Perkins, M. E., Voorhies, M. R., Harris, J. M., & Tucker, S. T., 2002, Environmental change in the Great Plains: an isotopic record from fossil horses: *Journal of Geology*, v. 110, p. 123-140.

Pearson, P. N. & Palmer, M. R., 2000, Atmospheric carbon dioxide concentrations over the past 60 million years: *Nature*, v. 406, p. 695-699.

Pedentchouk, N., Freeman, K. H., & Harris, N. B., 2006, Different response of δD values of *n*-alkanes, isoprenoids, and kerogen druing thermal maturation: *Geochimica et Cosmochimica Acta*. v. 70, p. 2063-2072.

Peters, K. E., Walters, C. C., & Moldowan, J. M., 2005, The Biomarker Guide: Volume 1, Biomarkers and Isotopes in the Environment and Human History: New York, Cambridge University Press, 492 p.

Poage, M. A. & Chamberlain, C. P., 2002, Stable isotopic evidence for a pre-Middle Miocene rain shadow in the western Basin and Range: Implications for the paleotopograhy of the Sierra Nevada. *Tectonics*. v. 21, 1-10.

Polissar, P. J. & Freeman, K. H., 2010, Effects of aridity and vegetation on plant-wax δD in modern lake sediments: *Geochimica et Cosmochimica Acta*, v. 74, p. 5785-5797.

Raymo, M. E., 1994, The Himalayas, organic carbon burial, and climate in the Miocene: *Paleoceanography*, v. 9, p. 399-404.

Retallack, G. J., 2007, Cenozoic paleoclimate on land in North America: *Journal of Geology*, v. 115, p. 271-294.

Retallack, G. J., 2009, Refining a pedogenic-carbonate CO_2 paleobarometer to quantify a middle Miocene greenhouse spike: *Palaeogeography, Palaeoclimatology, Palaeoecology*, v. 281, p. 57-65.

Rowley D.B. & Currie B.S., 2006, Palaeo-altimetry of the late Eocene to Miocene Lunpola basin, central Tibet: *Nature*, v. 439, p. 677-681.

Royer, D. L., Wing, S. L., Beerling, D. J., Jolley, D. W., Koch, P. L., Hickey, L. J., & Berner, R. A., 2001, Paleobotanical evidence for near present-day levels of atmospheric CO2 during part of the Tertiary: *Science*, v. 292, p. 2310-2313.

Sachse, D., Radke, J., Gleixner, G., 2004, Hydrogen isotope ratios of recent lacustrine sedimentary *n*-alkane record modern climate variability: *Geochimica et Cosmochimica Acta*. v. 68, p. 4877-4889.

Sachse, D., Radke, J., Gleixner, G, 2006, δD values of individual *n*-alkanes from terrestrial plants along a climatic gradient: implications for the sedimentary biomarker records: *Organic Geochemistry*. v. 37, p. 469-483.

Sachse, D., Kahmen, A., & Gleixner, G., 2009, Significant seasonal variation in the hydrogen isotopic composition of leaf-wax lipids for two deciduous tree ecosystems (*Fagus sylvativa* and *Acer pseudoplatanus*): *Organic Geochemistry*, v. 40, p. 732-742.

Sachse, D., Billault, I., Bowen, G. J., Chikaraishi, Y., Dawson, T. E., Feakins, S. J., Freeman, K. H., Magill, C. R., McInerney, F. A., van der Meer, M. T., Polissar, P., Robins, R., Sachs, J. P., Schmidt, H., Sessions, A. L., White, J., West, J. B., & Kahmen, A., 2012, Molecular paleohydrology: interpreting the hydrogen-isotopic composition of lipid biomarkers from photosynthesizing organisms: *Annual Review of Earth and Planetary Sciences*, v. 40, p. 221-249

Schefuß, E., Schouten, S., Jansen, J. F., & Damsté, J. S. S., 2003, African vegetation controlled by tropical sea surface temperatures in the mid-Pleistocene period: *Nature*, v. 422, p. 418-421.

Schimmelmann, A., Sessions, A. L., Mastalerz, M., 2006, Hydrogen isotopic (D/H) composition of organic matter during diagenesis and thermal maturation: *Annual Review of Earth and Planetary Sciences*, v. 34, p. 501-533.

Sessions, A. L., Sylva, S. P., Summons R. E., Hayes, J. M., 2004, Isotopic exchange of carbon-bound hydrogen over geologic timescales: *Geochimica et Cosmochimica Acta*. v. 68, p. 1545-1559.

Sheldon, N. D., 2006, Using paleosols of the Picture Gorge Basalt to reconstruct the middle Miocene climatic optimum: *PaleoBios*, v. 26, p. 27-36.

Shevenell, A. E., Kennett, J. P., & Lea, D. W., 2004, Middle Miocene southern ocean cooling and Antarctic cryosphere expansion: *Science*, v. 305, p. 1766-1770.

Skipp, B., Ruppel, E. T., Janecke, S. U., Perry Jr, W. J., Sears, J. W., Bartholomew, M. J., Stickney, M. C., Fritz, W. J., Hurlow, H. A., & Thomas, R. C., 2000, Geologic Map of the Lima 30′ X 60′ Quadrangle, Southwest Montana: Montana Bureau of Mines and Geology.

Smith, B. N., & Epstein, S.,1970, Biogeochemistry of the stable isotopes of hydrogen and carbon in salt marsh biota: *Plant Physiology*, v. 46, p. 738-742.

Solomon, S., Plattner, G. K., Knutti, R., & Friedlingstein, P., 2009, Irreversible climate change due to carbon dioxide emissions: *Proceedings of the national academy of sciences*, v. 106, p. 1704-1709.

Strömberg, C. A., 2005, Decoupled taxonomic radiation and ecological expansion of open-habitat grasses in the Cenozoic of North America: *Proceedings of the National Academy of Sciences of the United States of America*, v. 102, p. 11980-11984.

Strömberg, C. A. & McInerney, F. A., 2011, The Neogene transition from C3 to C4 grasslands in North America: assemblage analysis of fossil phytoliths: *Paleobiology*, v. 37, p. 50-71.

Tipple, B. J. & Pagani, M., 2007, The early origins of terrestrial C_4 photosynthesis: *Annual Review of Earth and Planetary Sciences*. v. 35, p. 435-461.

Tipple, B. J., Meyers, S. R., & Pagani, M., 2010, Carbon isotope ratio of Cenozoic CO2: a comparative evaluation of available geochemical proxies: *Paleoceanography*, v. 25, PA3202.

Tipple, B. J. & Pagani, M., 2010, A 35 Myr North American leaf-wax compound specific carbon and hydrogen isotope record: implications for C_4 grasslands and hydrologic cycle dynamics: *Earth and Planetary Science Letters,* v. 299, p. 250-262.

Tipple, B. J., Pagani, M., Krishnan, S., Dirghangi, S., Galeotti, S., Agnini, C., Giusberti, L., & Rio, D., 2011, Coupled high-resolution marine and terrestrial records of carbon and hydrologic cycles variations during the Paleocene-Eocene Thermal Maximum (PETM): *Earth and Planetary Science Letters*, v. 311, p. 82-92.

Tipple, B. J., Berke, M. A., Doman, C. E., Khatchaturyan, S., & Ehleringer, J., 2012, Leaf-wax *n*-alkanes record the plant water environment at leaf flush: *Proceedings of the National Academy of Sciences of the United States of America*, v. 110, p. 2659-2664.

Tipple, B. J. & Pagani, M., 2013, Environmental control on easter broadleaf forest species' leaf wax distributions and D/H ratios: *Geochimica et Cosmochimica Acta*, v. 111, p. 64-77.

Vincent, E. & Berger, W. H., 1985, Carbon dioxide and polar cooling in the Miocene: The Monterey hypothesis, *in* Sundquist, E. T. & Broecker, W. S., ed., The Carbon Cycle and Atmospheric CO: Natural Variations Archean to Present: Washington, D.C., American Geophysical Union, p. 455-468.

Wei, K. Y. & Kennett, J. P., 1986, Taxonomic evolution of Neogene planktonic foraminifera and paleoceanographic relations: *Paleoceanography*, v. 1, p. 67-84.

Welker, J. M., 2000, Isotopic ($\delta^{18}O$) characteristics of weekly precipitation collected across the USA: an initial analysis with application to water source studies: *Hydrological Processes*, v. 14, p. 1449-1464.

Wickman, F. E., 1952, Variations in the relative abundance of the carbon isotopes in plants: *Geochimicha et Cosmochimica Acta*, v. 2, p. 243-254.

Wolfe, J. A., 1985, Distribution of major vegetational types during the Tertiary, *in* Sundquist, E. T. & Broecker, W. S., ed., The Carbon Cycle and Atmospheric CO: Natural Variations Archean to Present: Washington, D.C., American Geophysical Union, p. 357-375.

Woodruff, F., 1985, Changes in Miocene deep-sea benthic foraminiferal distribution in the Pacific Ocean: Relationship to paleoceanography: *Geological Society of America Memoirs*, v. 163, p. 131-176.

Wright, J. D., Miller, K. G., & Fairbanks, R. G., 1992, Early and middle Miocene stable isotopes: Implications for deepwater circulation and climate: *Paleoceanography*, v. 7, p. 357-389.

You, Y., Huber, M., Müller, R. D., Poulsen, C. J., & Ribbe, J., 2009, Simulation of the middle Miocene climate optimum: *Geophysical Research Letters*, v. 36, L04702.

Zachos, J., Pagani, M., Sloan, L., Thomas, E., & Billups, K., 2001, Trends, rhythms, and aberrations in global climate 65 Ma to present: *Science*, v. 292, p. 686-693.

Zhang, J. W., & Cregg, B. M., 1996, Variation in stable carbon isotope discrimination among and within exotic conifer species grown in eastern Nebraska, USA: *Forest ecology and management*, v. 83, p. 181-187.

Zhang, J. W., Feng, Z., Cregg, B. M., & Schumann, C. M., 1997, Carbon isotopic composition, gas exchange, and growth of three populations of ponderosa pine differing in drought tolerance: *Tree physiology*, v. 17, p. 461-466.

Zhou, Y., Grice, Kliti, G., Stuart-Williams, H., Farquhar, G., Hocart, C., Lu, H., & Liu, W., 2010, Biosynthetic origin of the saw-toothed profile in $\delta^{13}C$ and $\delta^{2}H$ of *n*-alkanes and systematic isotopic differences between *n*-, *iso*- and *anteiso*-alkanes in leaf waxes of land plants: *Phytochemistry*. v. 71, p. 388-400.